THESIS

COMPARING SNOTEL SOIL MOISTURE PULSE AND SENTINEL-1 ESTIMATES OF SNOWMELT RUNOFF TIMING ACROSS THE WESTERN U.S.: IMPLICATIONS FOR RADAR REMOTE SENSING

Submitted by

Ally Detre

Department of Geosciences

In partial fulfillment of the requirements

For the Degree of Master of Science

Colorado State University

Fort Collins, Colorado

Summer 2025

Master's Committee:

Advisor: Daniel McGrath

Jessica O'Connell
Jeremy Rugenstein

ABSTRACT

COMPARING SNOTEL SOIL MOISTURE PULSE AND SENTINEL-1 ESTIMATES OF SNOWMELT RUNOFF TIMING ACROSS THE WESTERN U.S.: IMPLICATIONS FOR RADAR REMOTE SENSING

Satellite-based synthetic aperture radars (SAR) have been used to assess and quantify snowmelt across large spatial and temporal scales. Recent studies have utilized Sentinel-1 SAR to identify snowmelt runoff onset in high-elevation and variable terrain based on the seasonal minimum backscatter received by the sensor, however, C-band SAR sensitivity to physical changes in snowpack conditions across varying climatic regimes warrants further investigation. In this study, I integrated repeat field measurements, 260 SNow TELemetry (SNOTEL) stations across the western U.S., and paired Sentinel-1 SAR estimates of runoff generation to 1) assess how snowpack conditions evolved prior to and after Sentinel-1 SAR-derived runoff generation, and 2) evaluate Sentinel-1 SAR estimates of runoff generation with SNOTEL-derived estimates of melt output via soil moisture "pulses". I found that SNOTEL soil moisture pulses preceded Sentinel-1 SAR estimates of snowmelt runoff onset by a median 3 days (± standard deviation 25.3 days) and post-dated peak SWE by a median of 3 days (± standard deviation 18.2 days). Pulse dates occur latest at SNOTEL stations in maritime snowpacks and earliest in montane forests/prairie snowpacks. SNOTEL densities and number of positive degree days (PDD) on soil moisture pulse day of year (DOY) increased with latitude and longitude and decreased with elevation. Satellite-based estimates of melt onset provide a promising methodology for improving spaceborne retrievals of SWE, but my research emphasizes the importance and

influence of local climatological conditions on runoff onset signal quality for both in-situ and satellite-based estimates.

ACKNOWLEDGEMENTS

First and foremost, I would like to thank my advisor, Dr. Dan McGrath, for providing unparalleled mentorship, guidance, and direction and throughout my degree. I am incredibly grateful for this opportunity and the many valuable experiences that have come with it. Thank you to my committee members, Dr. Jessica O'Connell and Dr. Jeremy Rugenstein for their feedback and assistance in reviewing my work. To Dr. Randall Bonnell (USGS–Water Mission Area), thank you for your support throughout this entire process, I am so appreciative of your patience and generosity with your time and knowledge, you have undoubtedly made me a better scientist. To Eric Gagliano (University of Washington), thank you for your eager and continued collaboration in methods development. To Dr. H.P. Marshall (Boisie State University) and Dr. Ryan Webb (University of Wyoming), thank you for your advisement and expertise throughout this process. The research herein was funded by NASA Terrestrial Hydrology Award 80NSSC22K1113.

Fieldwork for this thesis was made possible by the assistance of Ashlesha Khatiwada, Kajsa Holland-Goon, Emi Patel, and Miranda Nestor. I would also like to acknowledge that fieldwork was conducted on the traditional and ancestral lands of the Arapaho, Cheyenne, and Ute Nations and peoples and recognize the indigenous peoples as original stewards of this land and all relatives within it.

To the CryoCrew: Randall, Lucas, Ash, Helen, and Noah, I am so grateful for your expertise and camaraderie. Days in the office and in the field, no matter how tough, were always fun and filled with laughs because of you all.

Last, but certainly not least, I would like to thank my family for their unwavering support of my passions and endeavors no matter what they might be. Mom, Dad, and Paul, I truly cannot thank you enough for everything you've done for me and for your encouragement, love, and sacrifices. Andie, thank you for your constant support throughout this degree and celebrating my successes, no matter how small, and for always being the voice of reason in my life. I did not forget to include your fieldwork contributions this time around. And finally, to my grandparents, Zsuzsanna, Zoltan, Tamás, and Katherine, thank you for blazing the trail so I could follow, I hope I've made you proud.

TABLE OF CONTENTS

LIST OF FIGURES

1. INTRODUCTION

1.1 Seasonal Snow Climatology Across the Western U.S.

Snow plays an integral role in the Earth's ecologic, hydrologic, and climate systems (Barnett et al., 2005; Campbell et al., 2005; Cohen & Entekhabi, 2001; Vavrus, 2007). In the northern hemisphere, snow occupies up to 63% of the land surface at its maximum extent (Barry & Gan, 2022; Hammond et al., 2018), and has a high albedo (reflectivity), with fresh snow reflecting 80–90% of incoming solar radiation (Warren, 1982). The significant spatial extent of snow cover combined with the highly reflective nature of snow are important for both regional and global climates (Déry & Brown, 2007; Groisman et al., 1994; Robock, 1983). Across the globe, mountainous regions serve as natural water towers (Immerzeel et al., 2020; Sarmiento, 2022; Viviroli et al., 2007), with mountain snowpacks contributing to 32% of global discharge (Meybeck et al., 2001) and providing critical water resources to ~1.2 billion people (Barnett et al., 2005). In North America alone, mountains account for approximately 25% of land area and contain ~60% of the continent's seasonal snow (Wrzesien et al., 2018).

Across the western U.S. snow accumulation and associated physical properties are highly variable, reflecting different winter precipitation patterns and characteristics. In maritime regions along the western coastline, accumulation patterns are dictated by wintertime atmospheric rivers that result in large magnitude snowfall events over short periods of time (Guan et al., 2010; Neiman et al., 2008). Conversely, snow accumulation in continental regions in the country's interior is dominated by low precipitation intensity frontal storms and colder air temperatures, resulting in long accumulation seasons (~months for mountains of Colorado) (Serreze et al., 1999; Trujillo & Molotch, 2014). As snow accumulates, it continues to undergo changes, metamorphosing and densifying as the season goes on (Seibert et al., 2021; Zhao et al., 2023)

and undergoes three general phases of melting (Dingman, 2015): moistening, ripening, and runoff (Figure 1). In the initial moistening phase, air temperatures and solar radiation increase, and surface layers of the snowpack begin to melt. The following ripening phase begins when maximum pore retention capacity is exceeded, caused by repeated cycles of melting and refreezing, and the snowpack becomes isothermal (Colbeck, 1977; Kattelmann & Dozier, 1999). At this point, when no additional liquid water can be retained, the snowpack begins to output melt and the runoff phase begins (Garvelmann et al., 2013; Revuelto et al., 2016). Current warming trends are predicted to result in earlier melt seasons (Barnett et al., 2005; Bales et al. 2006) and altered streamflow timing (Clow, 2010), and significantly decrease mountain snowpacks (Siirila-Woodburn et al., 2021). Water stored in the snowpack, or snow water equivalent (SWE), provides crucial resources for ecosystem health, and agricultural, hydroelectric, and outdoor recreation industries (Leathers et al., 2024; Marshall & Chen, 2022; Nolin & Daly, 2006; Qin et al., 2020).

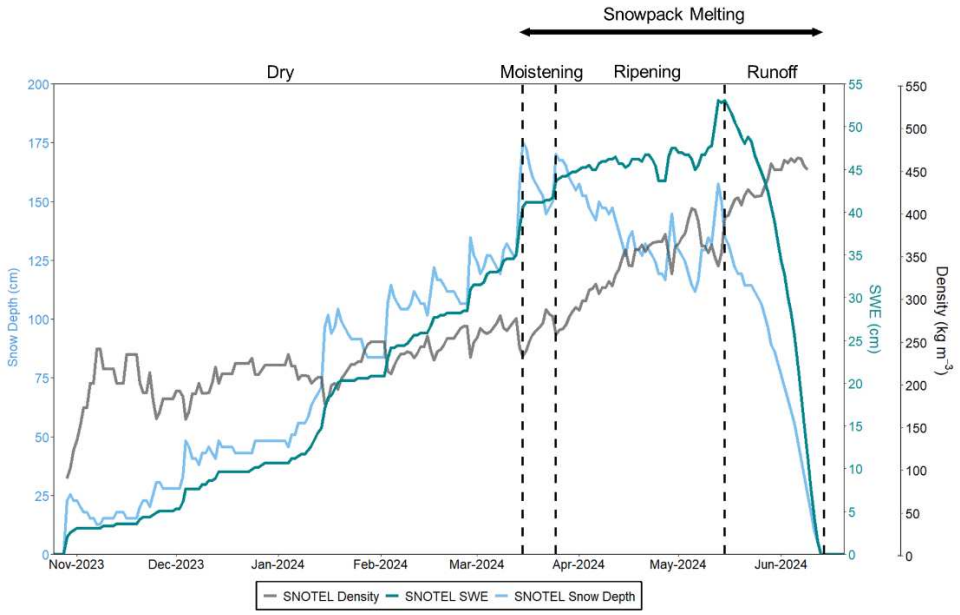

Figure 1: Example schematic of the temporal evolution of three phases of snowmelt (moistening, ripening, runoff) with SWE (cm), snow depth (cm), and snow density (kg m^{-3}) using data from 2023–2024 at the Hoosier Pass SNOTEL station located in Summit County, CO.

1.2 Snow Measurement and Observational Methods

Obtaining ground-based measurements of the snowpack throughout the accumulation and melt season are important for understanding snowpack conditions and evolution, as both snow accumulation and melt vary spatially and temporally depending on local climatological and topographic forcings (López-Moreno et al., 2013; Revuelto et al., 2014; Trujillo et al., 2007). Many options for ground-based measurements exist, and each has its own share of advantages and disadvantages. In-situ measurements made via snowpits (Figure 2) using handheld, portable sensors and tools provide accurate observations of snow depth, temperature, density, permittivity, grain size, hardness, wetness, and SWE for individual snow layers instead of a single bulk measurement at dispersed point locations throughout a given study area (Kinar & Pomeroy, 2015). Manual measurements of depth and SWE can also be collected along a survey

transect to cover a larger area (Kinar & Pomeroy, 2015), including snow course surveys conducted by the Natural Resources Conservation Service (NRCS) (or other agencies), which consist of repeated measurements of SWE and snow depths taken at pre-determined locations, either coincident with automated stations or stand-alone in remote locations (Osterhuber, 2014). Both snowpit and depth/SWE transects are snapshots of the snowpack state at their time of measurement.

Figure 2: Manually measuring snow density, depth, temperature, permittivity, grain size, hardness, wetness, and SWE for individual snow layers within a snowpit during the 2024 melt season.

Time-lapse photography has also been used to monitor snow depth and snow cover in remote locations on a continuous time scale (Garvelmann et al., 2013; Revuelto et al., 2016). Automated station networks, like the SNOw TELemetry (SNOTEL) network, which comprises over 900 stations across the western U.S. (Figure 3), provide continuous, dispersed point, bulk measurements of snow and meteorological conditions in remote and high elevation regions with

persistent snowpacks on a daily/hourly basis. However, interpolation between stations is required to estimate SWE, amongst other metrics, over a larger spatial scale, introducing various challenges and inaccuracies.

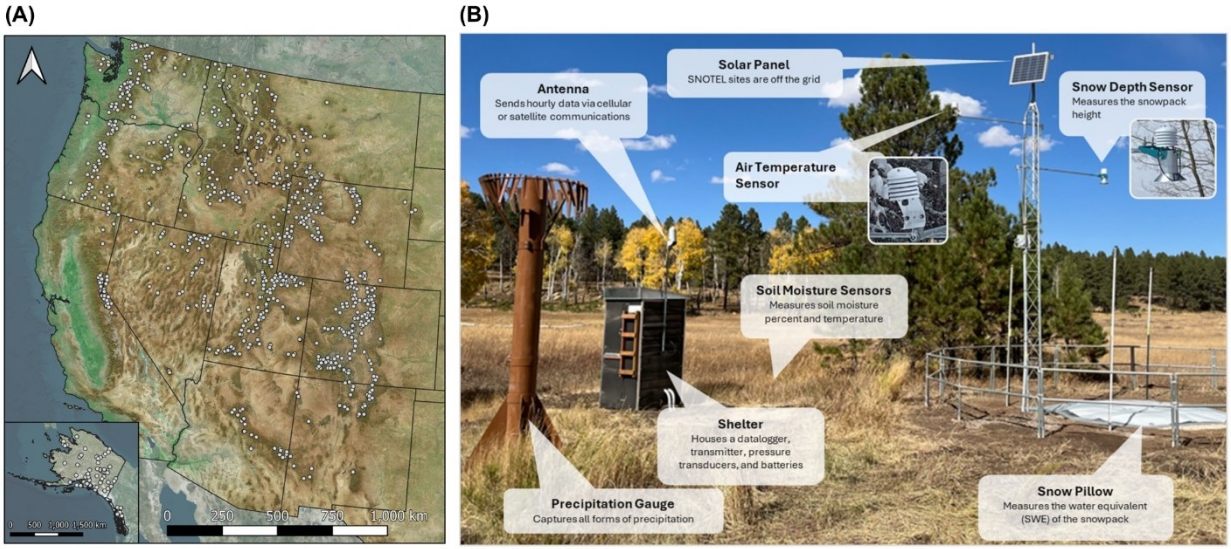

Figure 3: A) Map showing the extent of the SNOTEL station network across the western U.S. B) System architecture of a typical SNOTEL station designed to collect snowpack and related meteorological data. Photo courtesy of the NRCS.

1.3 Snow Modeling Approaches

Snow modeling approaches provide valuable snow cover and snow evolution estimates over larger spatial scales using automated station networks and existing field and precipitation data. Empirical snow models, like the degree-day model (Oerlemans, 1989; Rango & Martinec, 1995) use simple, statistically-based relationships with air temperature as the primary input. Conversely, physically based snow models are more complex and consider all energy flux exchanges at the snow surface. Both iSnobal and SnowModel are examples of complex, physically based modeling approaches that have been widely used across the western U.S.

(Hammond et al., 2023; Hedrick et al., 2018; Kumar et al., 2013; Meyer et al., 2023; Mower et al., 2024; Sourp et al., 2025). The iSnobal model simulates snowpack evolution by resolving both energy and mass balance fluxes for a given snowpack and timeseries, computing melt when accumulated energy exceeds the cold content of the snowpack (Marks et al., 1999; Meyer et al., 2023). SnowModel also simulates snowpack evolution, instead using four submodels to incorporate meteorological forcing, surface energy fluxes, snow depth/SWE/density changes, and snow redistribution by wind (Liston & Elder, 2006).

In addition to models, data assimilation products combine data from various sources, including spaceborne observations and ground-based measurements, with models to improve estimates of SWE, snow depth, and snow cover. SNODAS is one of these products, which provides daily estimates of snow cover, depth, SWE, and additional parameters in support of hydrologic modeling and analyses (Carroll et al., 2001). Similarly, the University of Arizona (UA) SWE gridded dataset provides daily SWE and snow depth estimates over the U.S. at a 4 km scale using assimilations of the SNOTEL and Nation Weather Service's Cooperative Observer Program (COOP) data (Broxton et al., 2016; Zeng et al., 2018). With multiple modeling and data assimilation products available, in addition to automated stations and spaceborne observations, methods for estimating snowpack evolution do not operate in isolation – the combination of a variety of methodologies is key to achieving the most accurate estimates of snowpack conditions that exhibit high degrees of spatial heterogeneity, especially in complex terrain environments.

1.4 Impacts of a Changing Climate on Seasonal Snowpacks

Snow serves as a vital hydrologic resource for both ecosystems and human populations throughout the western U.S. and across the world. Warming atmospheric temperatures and changing precipitation patterns due to climate change are altering the magnitude and timing of snow accumulation and melt. Since 1955, April 1 snow water equivalent (SWE) has declined at 90% of snow monitoring stations in the western U.S., accounting for a total loss of 15–30% (Mote et al., 2018). Current warming trends are predicted to significantly decrease mountain snowpacks this century and alter mountainous environments and ecosystems (Figure 4). Reduction in snow cover increases the surface area exposed to solar radiation, decreasing albedo and enhancing sensible heat flux, contributing to up to 2–4°C to future warming (Diro & Sushama, 2020; Liu et al., 2024). Streamflow is expected to decrease (Berghuijs et al., 2014) as temperatures rise, with winter precipitation more likely to shift from snow to rain (Kiewiet et al., 2022; Newton et al., 2021; Stewart, 2009). This phase change in future precipitation can result in less diffuse groundwater recharge in mountainous regions and a reduction in water storage (Earman et al., 2006; Meixner et al., 2016). Rising temperatures, combined with changing water availability due to snowpack loss, elevate evaporative demand (Condon et al., 2020; Hamlet et al., 2007) and can lead to changes in soil moisture regimes and ecosystem biodiversity (Blankinship et al., 2014; Wang et al., 2018).

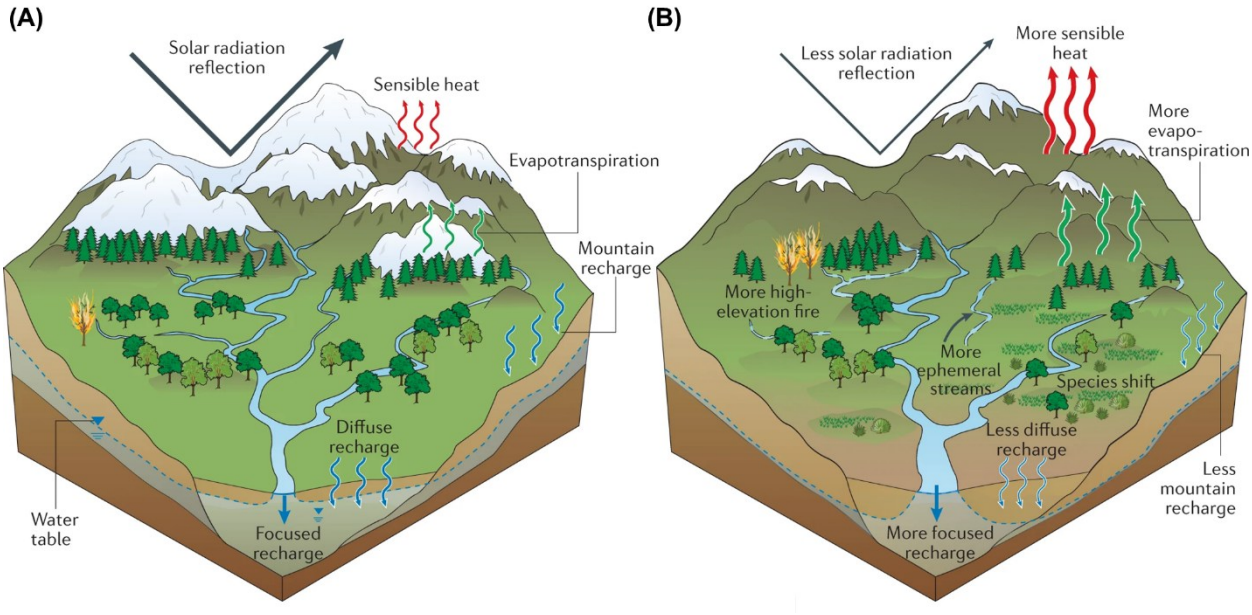

Figure 4: A) Schematic showing the physical and biological processes in mountain systems with seasonal snowpacks, and B) shifts in the physical and biological processes in mountain systems under future projections of decreasing mountain snowpacks. Figure from Siirla-Woodburn et al. (2021).

As a result of warmer temperatures, mid-winter melt is becoming more frequent (Musselman et al., 2021) and peak SWE timing has shifted eight days earlier per degree of warming (Kapnick & Hall, 2010), with SWE decline across the western U.S. projected to be ~25% ± 5% by 2050, ~35% ± 10% by 2075, and ~50% ± 10% by 2100 (Siirila-Woodburn et al., 2021). The loss of mountain snowpacks and decreasing SWE has and will result in earlier melt seasons (Barnett et al., 2005; Bales et al. 2006), and an earlier shift in streamflow timing on the order of weeks (Cayan et al., 2001; McCabe & Clark, 2005; Uzun et al., 2021). Altered streamflow and decreasing snowfall will cause reverberations in western U.S. hydrologic cycle and resources, as snowmelt is responsible for 53% of total runoff, accounting for 70% of total runoff in mountainous regions, and is expected to significantly decline by 2100 (Li et al., 2017). This cascade of effects, coupled with increased population growth in the western U.S., has

serious implications for the allocation and management of water resources as the climate continues to warm (Livneh & Badger, 2020; Stewart et al., 2004; Sturm et al., 2017), as the majority of the region's water supply is supported by snowmelt, especially in semi-arid basins (Li et al., 2017). Given the trajectory of warming trends and projected changes in snowmelt timing and decrease in snowpack storage, the ability to quantify SWE at high spatiotemporal scales across the globe is critical (Space Studies Board et al., 2019).

1.5 Snow Remote Sensing Methods

Many remote sensing methodologies are well-suited for the measurement of snow and SWE over larger spatial extents than station networks (Nolin, 2010). Optical remote sensing methods using sensors such as Landsat are useful in mapping the presence or absence of snow but are hindered by cloud and tree canopy cover (Klein et al., 1998; Nolin, 2010; Rittger et al., 2020). While passive microwave remote sensing platforms are able to measure SWE while penetrating canopy cover and atmospheric conditions on large spatial and temporal scales, the coarse spatial resolution of the large image footprint (km-scale) poses difficulties in making precise measurements (Foster et al., 2005), especially over heterogeneous terrain characteristic of mountainous regions (Awasthi & Varade, 2021). Airborne LiDAR can be used to measure snow depths at high spatial resolution (cm-scale) and accuracy (Deems et al., 2013; Painter et al., 2016) but can be cost-prohibitive at large spatial scales. Despite costs, Airborne Snow Observatories, Inc. (ASO) is using paired airborne LiDAR and imaging spectrometers to measure snow depth, albedo, and SWE across large river basins in the western U.S. The ASO works closely with the Colorado Airborne Snowpack Measurement (CASM) group, which is

working towards conducting regular ASO flights over the state of Colorado to provide improved streamflow forecasting.

Radar remote sensing is a promising approach for the estimation of snowmelt, wet snow conditions, snow depth, and SWE across large spatial and temporal scales. Synthetic aperture radar (SAR)-based methods are unique because microwave energy can penetrate clouds and depending on the frequency, canopy cover (Tsang et al., 2022). The Sentinel-1 constellation operated by the European Space Agency (ESA) carries C-band (5.405 GHz, ~5.55 cm wavelength) SAR and has been utilized to detect wet snow conditions based on backscatter change detection (Lund et al., 2022, 2023; Nagler et al., 2016), and to identify snowmelt runoff onset dates based on the seasonal minimum backscatter received by the sensor (Darychuk et al., 2023; Gagliano et al., 2023; Gao & Ma, 2024; Marin et al., 2020). In dry snowpacks, the primary source of backscatter is the interface between the snow and the ground, whereas in wet snowpacks the source of backscatter depends heavily on the amount and location of liquid water content (LWC) (Guneriussen et al., 2000; Jiancheng Shi & Dozier, 1995), as increased wetness causes high dielectric loss and reduced penetration depth of the radar signal (Matzler, 1987). Marin et al. (2020) and Gagliano et al. (2023) postulated that backscattered energy begins to decrease as the snowpack begins to contain water during the moistening and ripening phases, reaching a minimum when the snowpack becomes isothermal and saturated, causing runoff to begin, before increasing again when SWE begins to decrease (Dingman, 2015; Marin et al., 2020).

Recent developments have also shown that C- and L-band InSAR can be used to measure SWE over large areas and is similarly not hindered by cloud cover like other optical imaging methods (Bonnell et al., 2024; Oveisgharan et al., 2024; Palomaki & Sproles, 2023; Tarricone et

al., 2023)**.** With the launch of the NASA-ISRO SAR mission (NISAR) anticipated in 2025, L-band InSAR products will become publicly available at global scales, which is an exciting opportunity for the remote sensing of the cryosphere and snow-covered regions of the globe. Although promising, this methodology is highly sensitive to the presence of LWC in the snowpack during the melt season. The presence of LWC in the snowpack slows radar wave velocity given the high dielectric permittivity of water relative to dry snow and ice (Bradford et al., 2009), which can lead to inaccurate estimates of SWE (Bonnell et al., 2021). Thus, further investigation of the backscattered radar signal as it relates to the timing of the snowmelt season is necessary to further refine the applications of InSAR SWE retrievals.

1.6 Study Objectives

In this thesis, I integrate field measurements, automated stations, and Sentinel-1 estimates of snowmelt runoff onset to address two key questions: 1) How do snowpack characteristics (e.g., density, permittivity, temperature) evolve prior to and after Sentinel-1 SAR-derived snowmelt runoff onset? and 2) What is the temporal lag between Sentinel-1 SAR-derived estimates of snowmelt runoff onset and SNOTEL-derived estimates of melt output via soil moisture “pulses”? The comparison between ground-based measurements of the snowpack and spaceborne estimates of melt onset across multiple climatic regions will provide valuable insight into the processes leading up to snowmelt runoff onset and contribute to the development of more accurate SWE retrievals using radar-based methods.

2. METHODS

I evaluated Sentinel-1 SAR retrievals of backscatter minima with repeated field observations collected during the 2024 melt season at five SNOTEL sites. I expanded this study to include 260 SNOTEL stations spanning 2015–2024 (1,204 station-years) to further assess the timing and development of snowmelt across the western U.S. A summary of the methods is provided in Figure 5 and further details below.

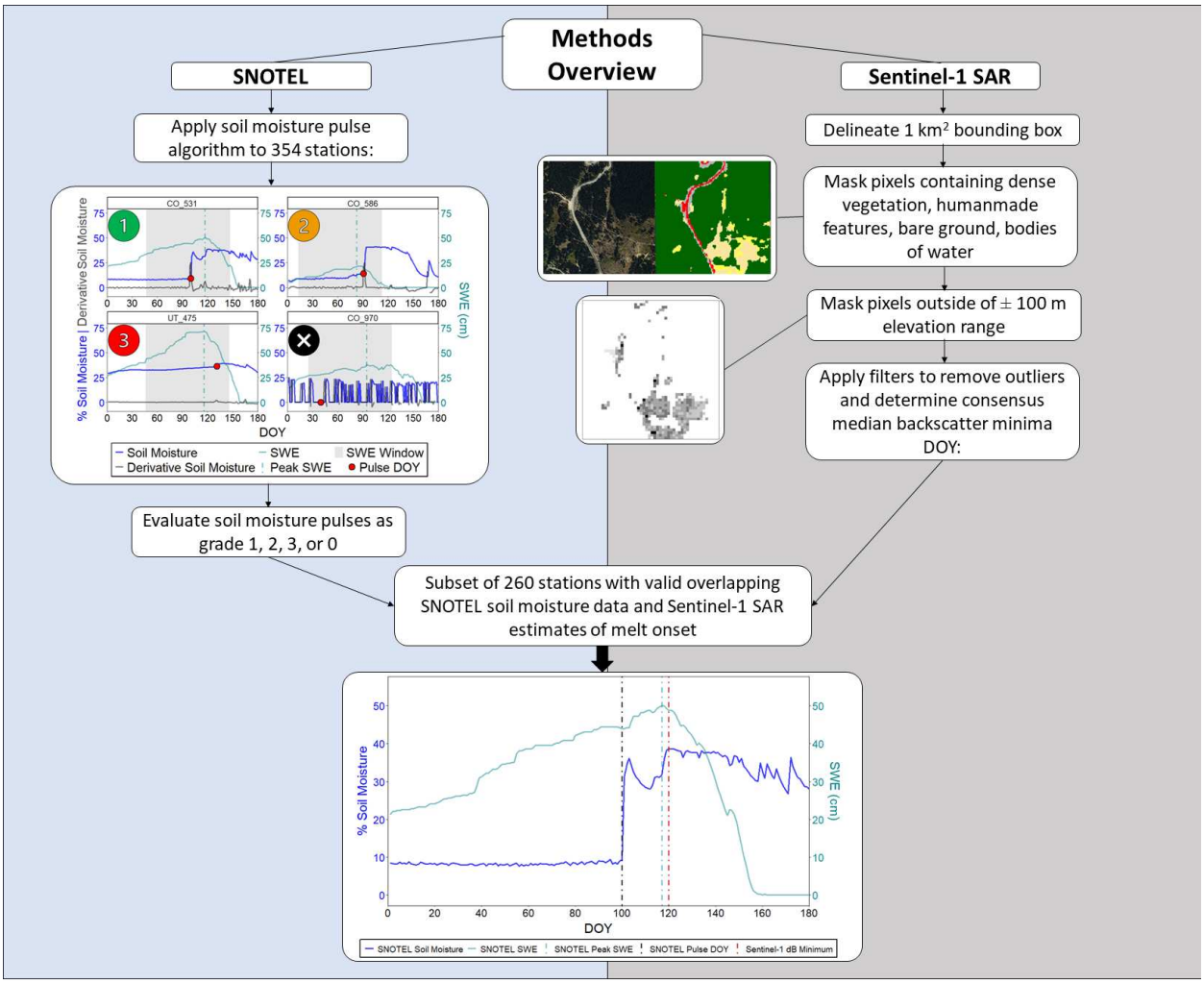

Figure 5: Methods flowchart detailing retrieval and processing workflows of both SNOTEL melt output via soil moisture pulse DOY (left) and Sentinel-1 SAR-derived estimates of snowmelt runoff onset via backscatter minima (left) for 260 sites.

2.1 Field Methods

I collected biweekly field observations proximal to five SNOTEL stations in Summit County, Colorado, U.S. at varying elevations during the 2024 melt season to evaluate snowpack properties. Surveyed SNOTEL sites include Berthoud Summit (CO_335), Fremont Pass (CO_485), Grizzly Peak (CO_505), Hoosier Pass (CO_531), and Summit Ranch (CO_802) (Figure 6). Following the Sturm & Liston (2021) classifications, the Hoosier Pass and Berthoud

Pass sites are located in the boreal forest snow classification, Fremont Pass and Grizzly Peak are classified as tundra, and Summit Ranch is classified as montane forest. The Hoosier Pass, Berthoud Pass, Fremont Pass, and Grizzly Peak sites are located between 3,442–3,535 m, while the lowest elevation site, Summit Ranch, is located at 2,850 m. All sites are on north-facing slopes, apart from Hoosier Pass (west-facing) and Summit Ranch (east-facing).

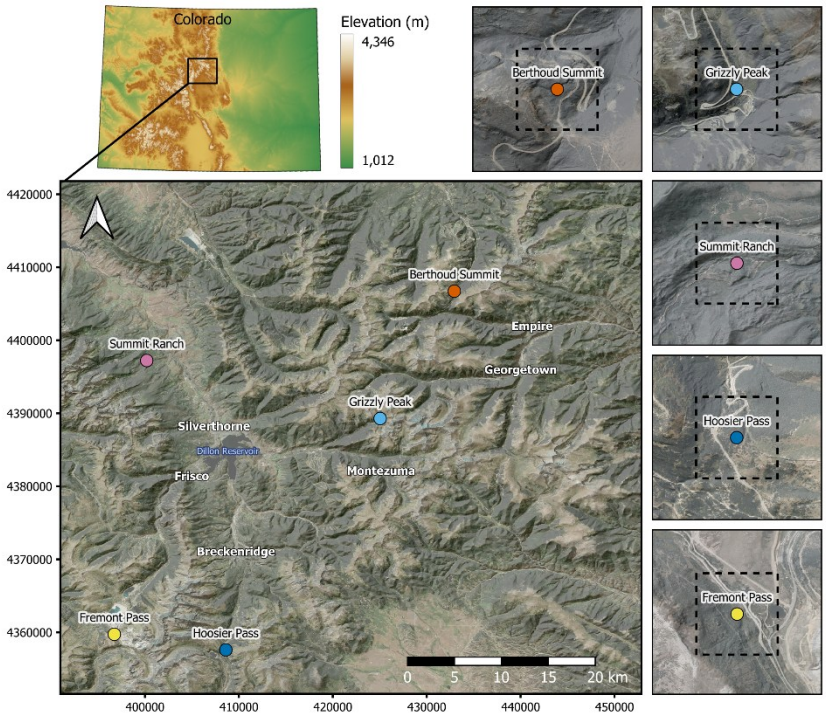

Figure 6: Locations of the five SNOTEL field sites in Summit County, Colorado. 1 km^2 Sentinel-1 SAR retrieval bounding boxes are delineated with black dashed lines in the inset images.

Hoosier Pass served as the control site and snowpack measurements were taken as close to the Sentinel-1 SAR overpass time as possible (either 06:00 or 18:00 Mountain Time). Surveys coincided with Sentinel-1 overpasses for the 2024 melt season, where snow depth, density, temperature, permittivity, and manual wetness were recorded. Snow density was measured in two vertical columns using a 1,000 cm^3 wedge cutter at 10 cm intervals. Snow temperature was

measured in a single vertical column with a digital thermometer with ± 0.5 °C accuracy at 10 cm intervals. I compared two permittivity sensors for snowpit observations: A2 WISe sensor developed by A2 Photonic Sensors and the SLF Snow Sensor developed by the Swiss Federal Institute for Snow and Avalanche Research. Permittivity measurements with both sensors were taken in two vertical columns at the midpoint of the 10 cm intervals. I found a close agreement between sensor observations (Figure 7) and thus only present the results of the A2 WISe sensor in figures.

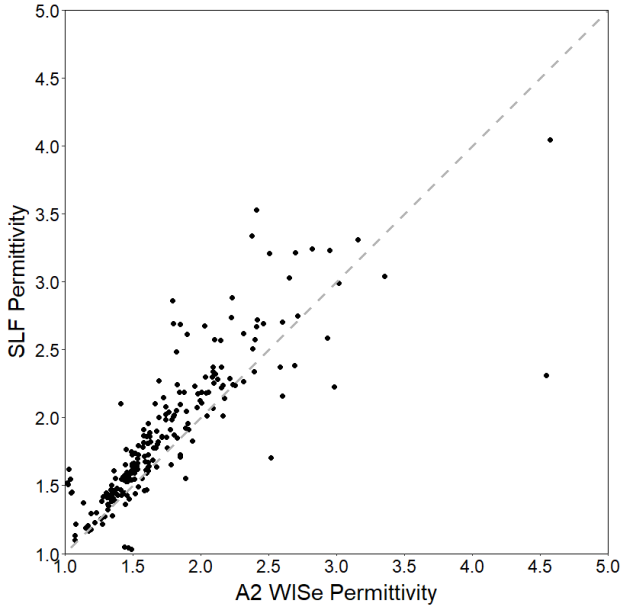

Figure 7: Scatterplot comparing paired measurements of permittivity using the A2 WISe sensor and SLF Snow Sensor during the 2024 melt season at five field sites in Summit County, CO (R^2 = 0.7 and RMSE = 0.29). SLF Snow Sensor measured permittivity was on average 0.12 higher than paired A2 WISe measured permittivity.

2.2 SNOTEL Methods

The SNOTEL network (Fleming et al., 2023) is comprised of over 900 stations across the western U.S. that make automated data collection at high elevation watersheds possible and accessible through a central database managed by the Natural Resource Conservation Service

(NRCS). SNOTEL stations provide hourly point observations of air temperature, precipitation, snow depth, and SWE. A subset of SNOTEL stations provide additional observations, including soil moisture. I accessed the 354 SNOTEL stations across the western U.S. that report soil moisture data from 2015–2024, but used stepwise filtering (see Section 2.3) to reduce to a subset of 260 SNOTEL stations (Figure 23) that have valid Sentinel-1 SAR estimates of snowmelt runoff onset. These stations range in elevation from 1,073 m to 3,353 m, span 14 Level-3 ecoregions (U.S. Environmental Protection Agency, 2013), 14 degrees of latitudes, 19 degrees of longitudes, and five snow classifications (Sturm & Liston, 2021). In order to facilitate the most direct comparison between the SNOTEL observations and Sentinel-1 retrievals, I utilized high-resolution optical imagery in Google Earth Pro to find more precise locations for these SNOTEL stations (median distance offset = 377 m, mean distance offset = 370 ± standard deviation 153 m, elevation offset = 9 ± standard deviation 57 m).

Each of these stations include multiple Stevens Hydraprobe soil moisture sensors at a variety of different depths (ranging from 5 to 100 cm where possible), which measures the dielectric constant and relative permittivity of the soil to determine moisture content (percent). Soil moisture was used as a proxy for snowmelt output at SNOTEL stations. The observed rapid increase in soil moisture was defined as the "pulse" associated with meltwater output from the snowpack into the soil. I identified the day of year (DOY) on which the first soil moisture pulse occurs as the first day on which the 2-day rate of soil moisture change exceeded 1.25 * the standard deviation of the rate of change. This method eliminates minor fluctuations and noise in the soil moisture timeseries to more correctly identify the first pulse. Pulse dates were restricted to occur within 70 days before and 30 days after the date of peak SWE. This window was selected based on results from a preliminary analysis of distance between pulse date from date of

peak SWE on a subset of SNOTEL stations that found that 95% of pulse dates were within 70 days before and 30 days after the date of peak SWE. The soil moisture pulse detection algorithm, amongst other SNOTEL station data processing tools and scripts can be found in the snotelprocessr package (Detre, 2025). All soil moisture pulse dates were visually evaluated and manually adjusted to optimize pulse consistency across all observations. Soil moisture pulses were assigned grades based on the quality of the pulse. I define Grade 1 pulses as having a distinct, single pulse corresponding to a sharp increase in soil moisture, a Grade 2 as a more gradual pulse, often associated with a smaller magnitude pulse occurring prior to a larger magnitude pulse, a Grade 3 as a low-confidence pulse, where the soil moisture timeseries had little to no fluctuation or discernable increase, and Grade 0 as unusable data, when there was too much non-real noise in the soil moisture signal or peak SWE < 15 cm (Figure 5)

For each SNOTEL station, there is a maximum of nine years of overlapping soil moisture and Sentinel-1 observations between 2015 and 2024. I define a "station-year" (e.g. station CO_531, year 2015 = 1 station year), yielding a total of 2,888 potential station-years. Of the potential station-years, 36% (n=846) were Grade 1, 29% (n=683) were Grade 2, 19% (n=434) were Grade 3, and 15% (n=925) were Grade 0 and were discarded. For the purposes of this research, only Grade 1 and 2 pulses were included in analyses.

Positive Degree Days (PDD) were calculated for each SNOTEL station-year soil moisture pulse DOY by taking the fractional sum of hourly air temperatures greater than 0 °C on each day and taking the cumulative sum of those values across the season. The Degree Day Model (Wake & Marshall, 2015) is a methodology commonly used in tracking glacier ablation and takes into account the amount of energy available for melt and assumes that for each 1°C over 0°C, a certain depth of snow will be melted. Similarly, SNOTEL snow density was

extracted on each station-year soil moisture pulse DOY and was used with calculated PDD to evaluate LWC development and snowpack evolution.

2.3 Sentinel-1 SAR Methods

The ESA Sentinel-1 mission originally consisted of two C-band SAR satellites (5.405 GHz) with a spatial resolution of 5 m x 20 m in Interferometric Wide mode with a combined orbital repeat pass cycle of ~6 days over the western U.S with descending and ascending overpasses at approximately 06:00 and 18:00 local time. Sentinel-1B's sensor ceased working in December 2021, leaving Sentinel-1A as the only operational satellite in the constellation until the launch of Sentinel-1C in 2025. Thus, from December 2021, the orbital repeat pass cycle increased to ~12 days. Some locations are covered by overlapping Sentinel-1 SAR orbital passes, decreasing the length of time between acquisitions.

All available radiometrically terrain corrected (RTC) measurements of backscatter across multiple orbital paths were accessed from the Microsoft Planetary Computer using a publicly accessible STAC API (Microsoft Open Source, 2022). I adapted open-source code from Gagliano (2022) to create an automated workflow (Figure 5) to generate composite snowmelt runoff onset DOY rasters for 260 SNOTEL stations across the western U.S between 2015 and 2024. A 1 km^2 bounding box centered around each SNOTEL station was generated with a corresponding USGS 3DEP digital elevation model (DEM) at 10 m resolution (United States Geological Survey, 2021). The melt season and Sentinel-1 search window were defined as 1 January through 1 August for years 2015 through 2024 (excluding 2016 due to coverage issues)

in order to capture the full extent of the melt season at stations located within a range of latitudes.

I estimated snowmelt runoff onset dates by identifying the median DOY of backscatter minima (Darychuk et al., 2023; Gagliano et al., 2023; Marin et al., 2020) for the pixels included in the 1 km^2 boundary, utilizing multiple polarizations (VV and VH) and both ascending and descending passes. Backscatter minima is assumed to occur at the end of the ripening phase and the beginning of the runoff phase, when the snowpack has become saturated and isothermal, and melt output begins, indicated by a decrease in SWE (Dingman, 2015). It is important to note that melt output via SNOTEL soil moisture and melt detected by Sentinel-1 SAR can reflect different stages in snowpack evolution. Previous studies (Lund et al., 2022; Manickam & Barros, 2020; Nagler et al., 2016) have utilized Sentinel-1 SAR thresholding approaches to detect surface melt. I elected to use the backscatter minima approach (e.g., Marin et al., 2022, Gagliano et al., 2023) in this study as an estimate of snowmelt runoff onset, as this is most closely aligned with the in-situ measurements of melt output via SNOTEL soil moisture pulses.

Pixels containing dense vegetation cover, humanmade structures, and bodies of water were masked using the ESA Worldcover v100 land cover classification product at 10 m resolution (Zanaga, 2021). Pixels that exceeded ±100 m elevation range from the elevation of the SNOTEL station were further masked. To remove early/late season outliers, I defined the period for potential melt output as the period between the first and last instance of 50% peak SWE. Additional stepwise filtering was applied to remove outliers and determine a consensus backscatter minima DOY for each station-year: first, I ensured that each orbital pass contained greater than four acquisition dates and the backscatter range was greater than 1.25 dB. To capture potential backscatter minima DOY where melt output was possible, only backscatter

acquisitions with same-day SNOTEL-measured maximum air temperature > 0 °C were considered for the calculation of median backscatter minimum. After applying the series of filters for quality assurance, the result was 1,204 station-years with matching SNOTEL soil moisture pulse data.

3. RESULTS

3.1 In-Situ Evaluation of Snowmelt Development Throughout the 2024 Melt Season

Over the course of the 2024 melt season, I surveyed five field sites in Summit County, Colorado at varying elevations to assess the temporal evolution of density, temperature, and permittivity. The Hoosier Pass site was the control site, with snowpack measurements taken as close to the approximate Sentinel-1 SAR overpass time as possible. All snowpit measurements were taken during the ascending (approximately 18:00 MST) overpass except for the dry snow survey on 2 March, which was taken with the descending (approximately 06:00 MST) overpass. Snowpit measurements document increases in permittivity (related to density and LWC development) and temperature as the snowpack progresses from dry and cold to wet and isothermal (Figure 8). Median permittivity increased from 1.4 (dry snow) to 1.8 from pre- to post-soil moisture pulse. Median snowpack temperatures increased from –3.6 °C on the March 2 (DOY 62) survey to 0 °C by the April 14 survey (DOY 105), indicating that the snowpack was isothermal by this date, if not before. The soil moisture pulse at the nearby Hoosier Pass SNOTEL station occurred on DOY 105 and lagged approximately 10 days after the first > 0 °C air temperature period and preceded peak SWE by 29 days. After the pulse, SNOTEL soil moisture increased from approximately 10% to 36% over 3 days (Figure 8a). Average snowpit density increased from 285 kg m^{-3} on March 2 to 462 kg m^{-3} on 1 June (Figure 8b).

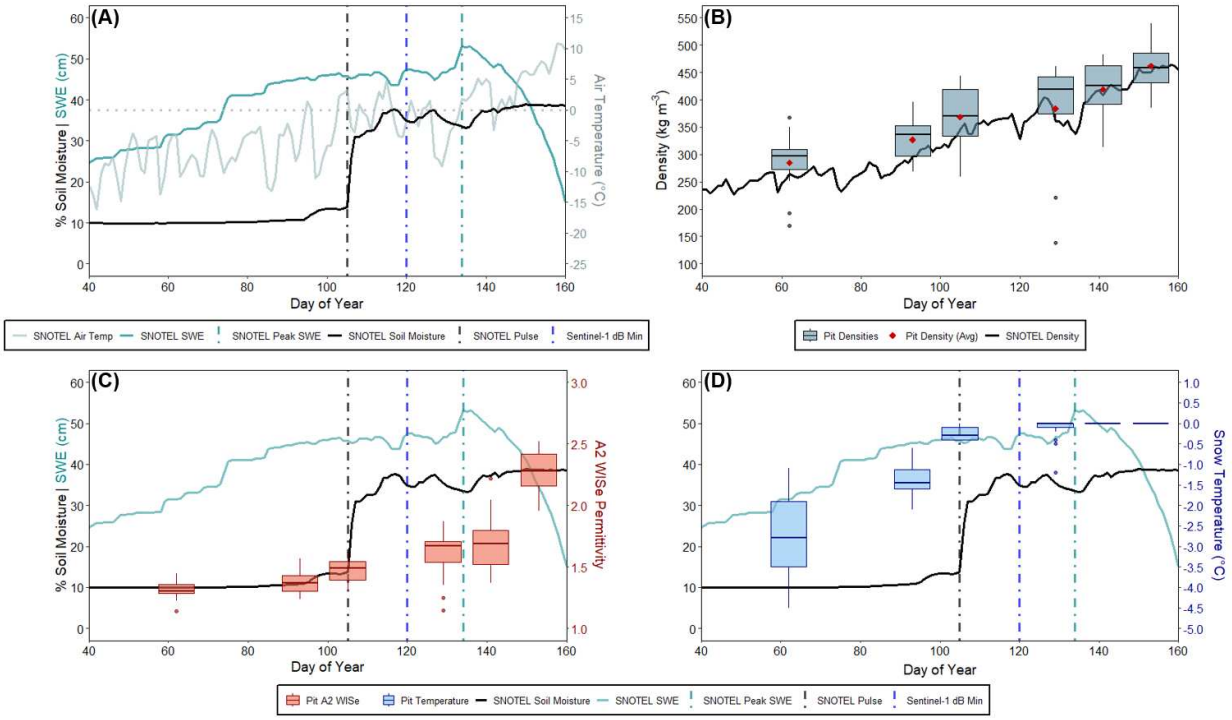

Figure 8: SNOTEL and pit observations over the 2024 melt season at Hoosier Pass SNOTEL station in Summit County, CO. A) SNOTEL metrics of soil moisture (%, 5 cm depth), SWE (cm), and air temperature (average, °C). B) SNOTEL density (kg m^{-3}) plotted with layer-averaged pit densities (kg m^{-3}) and average pit densities (red). C) Measurements of layer-averaged pit permittivity using the A2 WISe sensor and D) pit snow temperatures (°C).

Across all five field sites (Figures 8–12), the dry snow surveys (1–2 March) yielded an average density of 285 ± 60.7 kg m^{-3}, an average permittivity of 1.3 ± 0.17 (0% vol. LWC), and an average snowpack temperature of –3.9 ± 2.8 °C. The final surveys on 1 June yielded an average density of 463 ± 38.1 kg m^{-3}, an average permittivity of 2.5 ± 0.54 (3.5% vol. LWC), and an average snowpack temperature of 0 °C. Soil moisture pulse dates for the accompanying SNOTEL stations at the Hoosier Pass, Berthoud Pass (Figure 9), and Fremont Pass (Figure 10) sites were DOY 105, 104, and 116, respectively. All three SNOTEL stations and adjacent snowpit measurements are located in meadows and between 3,442–3,535 m in elevation.

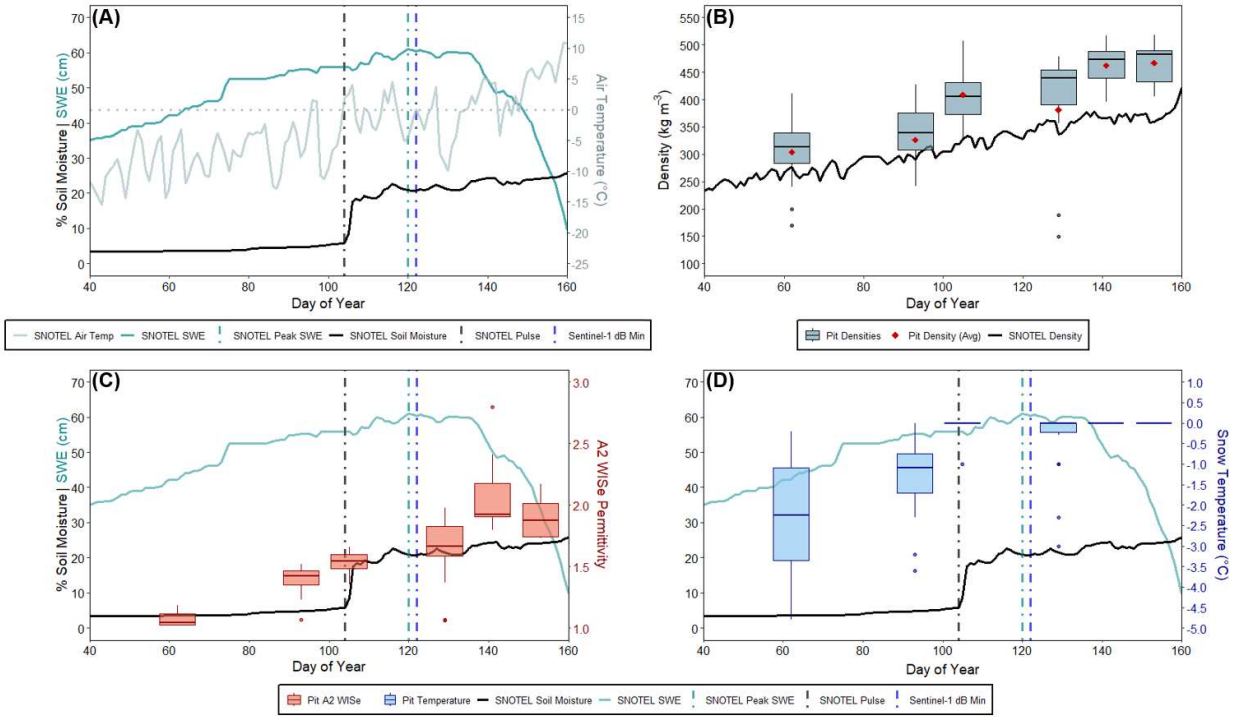

Figure 9: SNOTEL and pit observations over the 2024 melt season at Berthoud Pass SNOTEL station in Summit County, CO. A) SNOTEL metrics of soil moisture (%, 5 cm depth), SWE (cm), and air temperature (average, °C). B) SNOTEL density (kg m^{-3}) plotted with pit densities (kg m^{-3}) and average pit densities (red). C) Measurements of pit permittivity using the A2 WISe sensor and D) pit snow temperatures (°C).

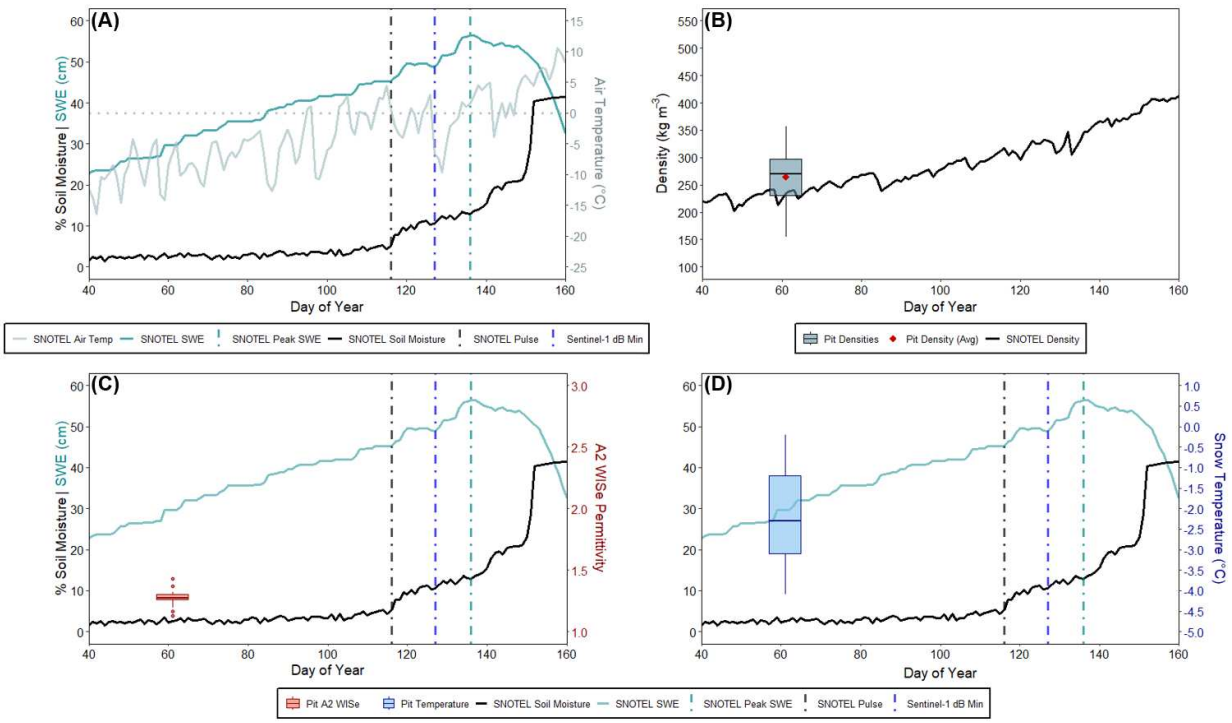

Figure 10: SNOTEL and pit observations over the 2024 melt season at Fremont Pass SNOTEL station in Summit County, CO. Only one survey (1 March) was conducted at Fremont Pass due to challenges related to site accessibility during the winter. A) SNOTEL metrics of soil moisture (%, 5 cm depth), SWE (cm), and air temperature (average, °C). B) SNOTEL density (kg m^{-3}) plotted with pit densities (kg m^{-3}) and average pit densities (red). C) Measurements of pit permittivity using the A2 WISe sensor and D) pit snow temperatures (°C).

The Grizzly Peak (Figure 11) site (at 3,387 m elevation) had a soil moisture pulse DOY of 148 and is located in an area with the densest forest cover of the five field sites. Due to the soil moisture timeseries having little to no fluctuation or discernable increase, I was not able to confidently detect a soil moisture pulse for the Summit Ranch (Figure 12) site. The Summit Ranch site is located within a deciduous forest at 2,850 m, 604 m lower on average than the other four field sites. Peak SWE occurred on DOY 95, while field observations showed that the snowpack was isothermal by DOY 93 (a minimum of 12 days earlier on average than the other field sites), suggesting that the soil moisture pulse date would have been the earliest of the five.

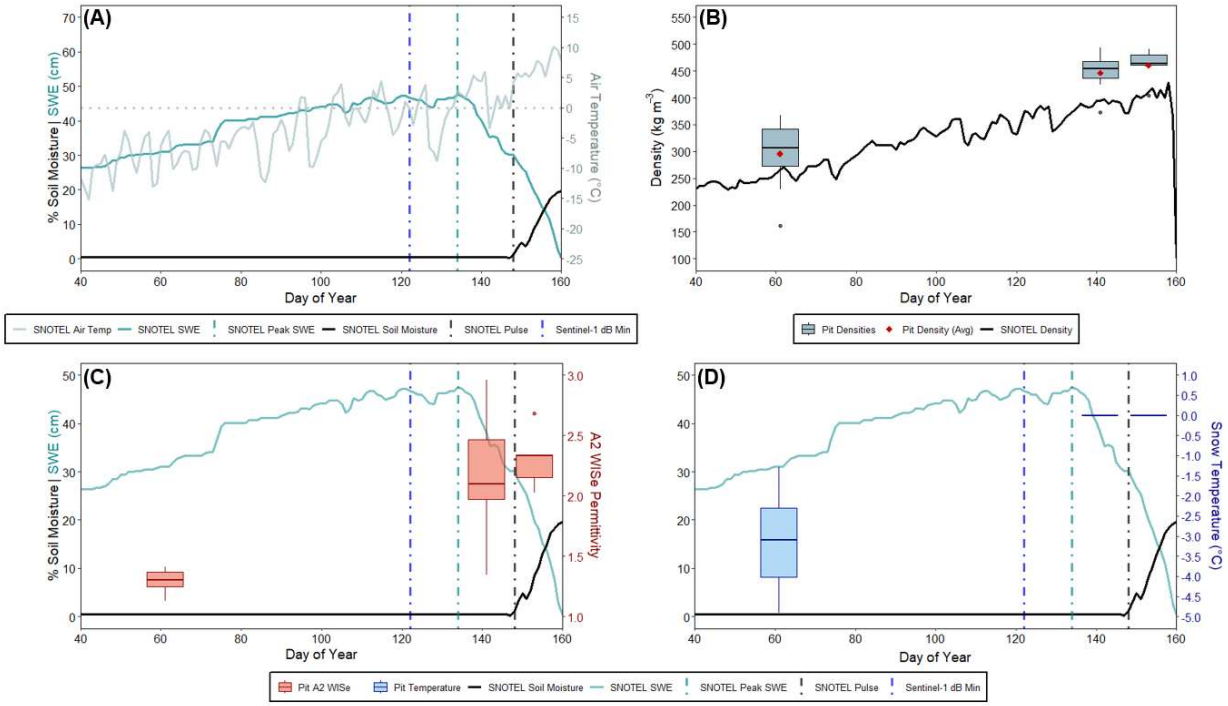

Figure 11: SNOTEL and pit observations over the 2024 melt season at Grizzly Peak SNOTEL station in Summit County, CO. The gap in field surveys is a result of challenges related to site accessibility during the winter. A) SNOTEL metrics of soil moisture (%, 5 cm depth), SWE (cm), and air temperature (average, °C). B) SNOTEL density (kg m^{-3}) plotted with pit densities (kg m^{-3}) and average pit densities (red). C) Measurements of pit permittivity using the A2 WISe sensor and D) pit snow temperatures (°C).

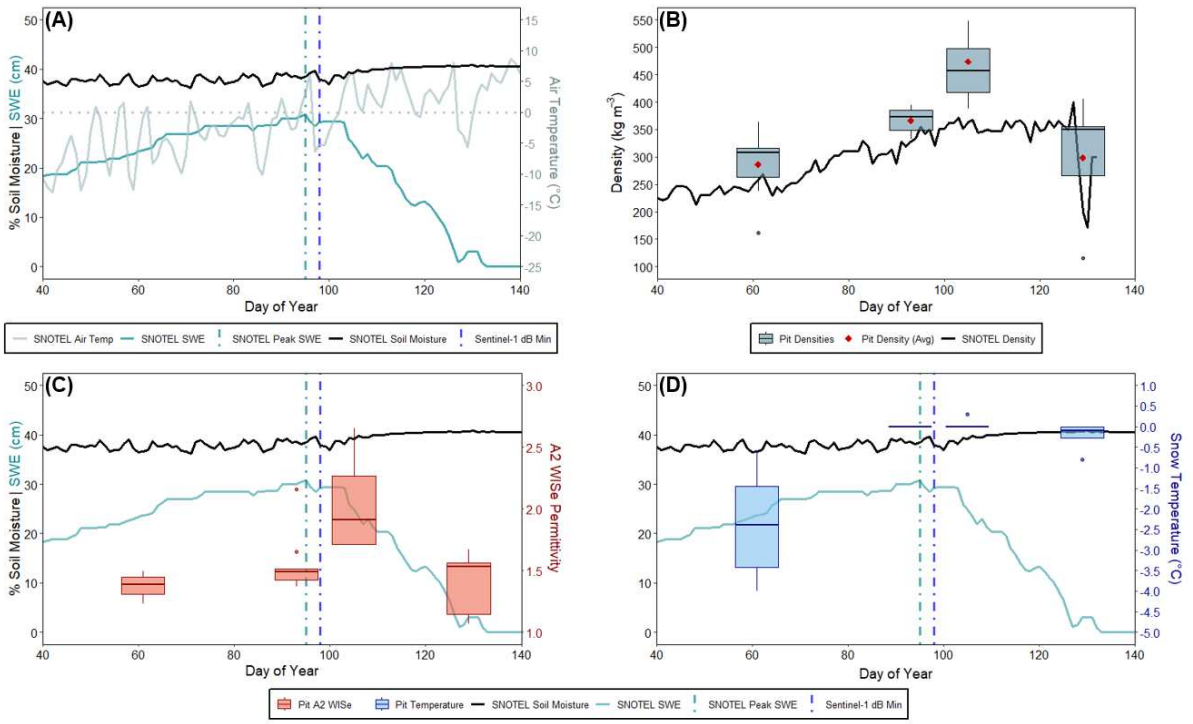

Figure 12: SNOTEL and pit observations over the 2024 melt season at Summit Ranch SNOTEL station in Summit County, CO. A) SNOTEL metrics of soil moisture (%, 5 cm depth), SWE (cm), and air temperature (average, °C). B) SNOTEL density (kg m^{-3}) plotted with pit densities (kg m^{-3}) and average pit densities (red). C) Measurements of pit permittivity using the A2 WISe sensor and D) pit snow temperatures (°C).

3.2 SNOTEL-Derived Estimates of Snowmelt Runoff Onset via Soil Moisture

The majority (n = 226, 87%) of SNOTEL stations used in this study are between 2,000-3,500 m in elevation. Stations between 2,000–3,500 m have a median soil moisture pulse DOY range of 91–101(1 April – 11 April). Pulse dates occurred latest at SNOTEL stations in maritime snowpacks (Figure 13), at an average DOY of 113 (median 116, ± 25 days), followed by boreal forest and tundra snow classes, occurring at an average DOY of 103 (median 101, ± 19 days) and 101 (median 99, ± 26 days), respectively. Pulse dates occurred earliest in montane forests at an average DOY of 92 (median 94, ± 19 days) and prairie snowpacks at an average DOY of 96 (median 95, ± 20 days). I did not observe strong trends related to elevation, latitude, or longitude.

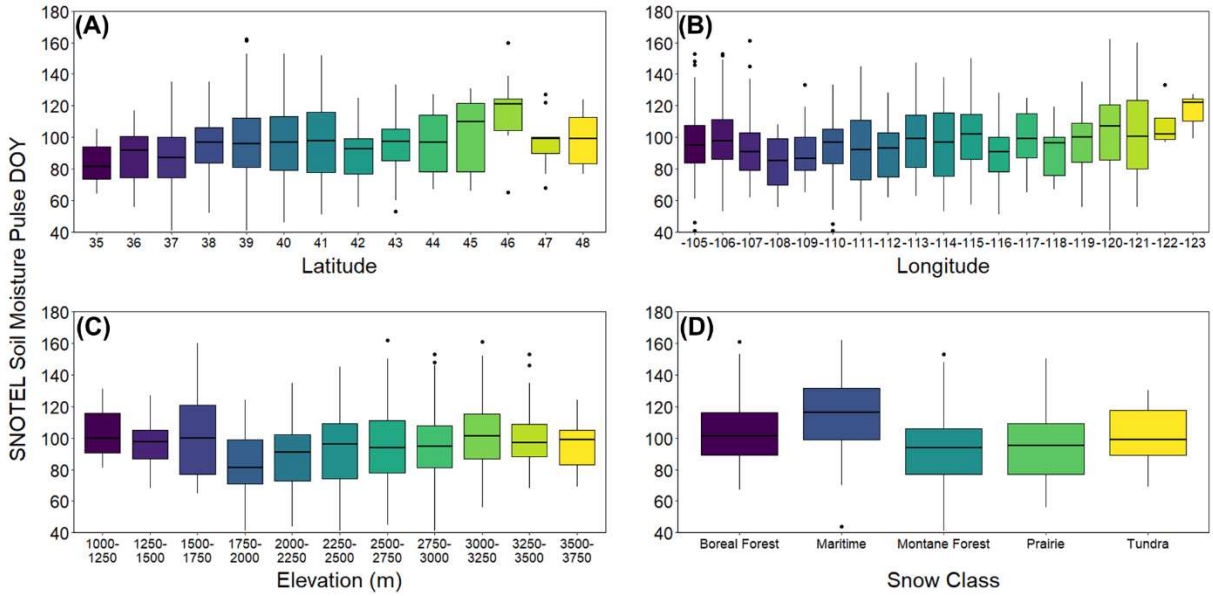

Figure 13: SNOTEL soil moisture pulse DOY by A) latitude, B) longitude, C) elevation, and D) snow class.

In evaluating the proximity of the SNOTEL soil moisture pulse DOY to peak SWE DOY (Figure 14), soil moisture pulses occurred an average of 0.8 ± 18.2 days and a median of three days after peak SWE. SNOTEL soil moisture pulses occur at an average of 88% (median 92% of peak SWE, standard deviation of ±13%) of peak SWE, which remained fairly consistent across all latitudes, longitudes, and elevations (Figure 15) except for the lowest elevation bin (n = 3, 1,000–1,250 m), which saw soil moisture pulses occur at an average of 84% of peak SWE. The tundra snow class reported pulses occurring at the highest percentage of peak SWE at an average of 91% (± 12%, median of 94%), while boreal forest, prairie, and montane forest reported pulses occurring at averages of 89% (± 10%), 88% (± 13%), and 87% (± 14%) peak SWE, respectively, with a median of 92%. The maritime snow class reported the lowest percentage, with an average of 85% (±14%) and median of 89% peak SWE. Within the elevation range of (2,000–3,500 m), the median peak SWE DOY is between DOY 91 and 111 (1 April – 21 April).

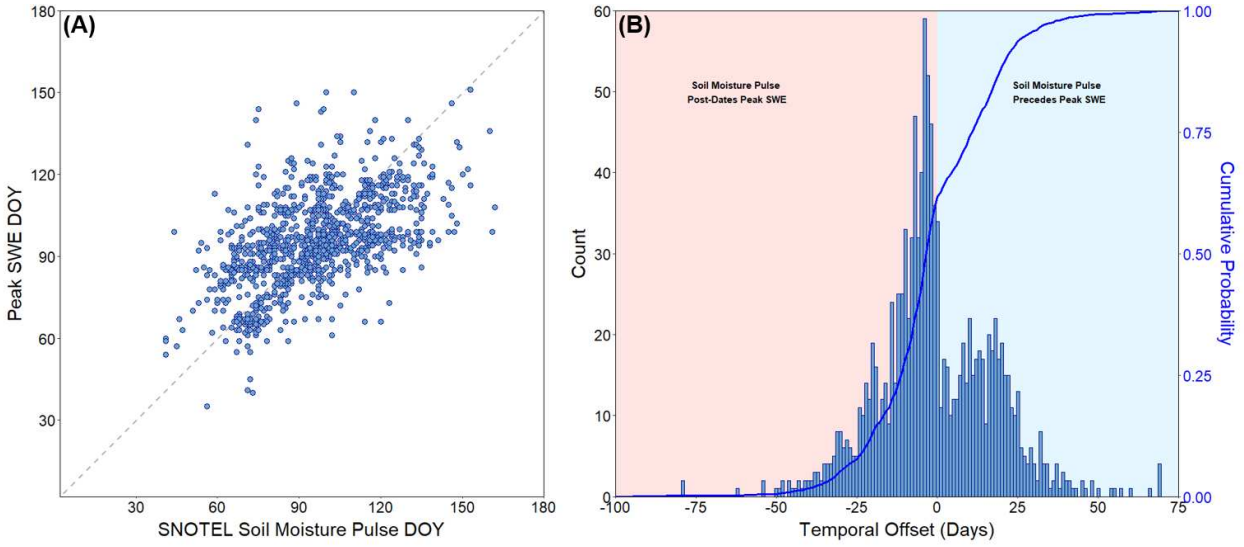

Figure 14: Paired A) scatterplot showing the relationship between peak SWE DOY and SNOTEL soil moisture pulse DOY (R^2 = 0.3, RMSE = 14.0 days), and B) histogram of the temporal offset (days) between peak SWE DOY and soil moisture pulse DOY, with corresponding cumulative probability curve (blue). Negative values (shaded in red) indicate soil moisture pulse DOY post-dates peak SWE DOY, while positive values (shaded in blue) indicate soil moisture pulse DOY precedes peak SWE DOY.

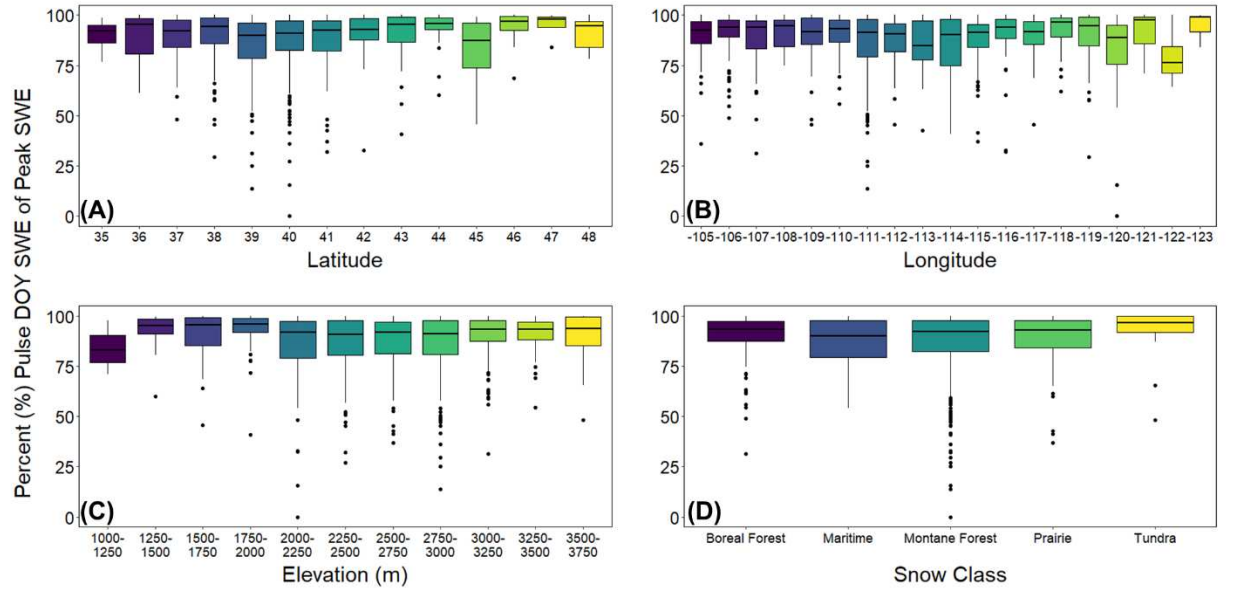

Figure 15: Percent (%) peak SWE on SNOTEL soil moisture pulse DOY by A) latitude, B) longitude, C) elevation, D) snow class.

PDD and snow density were evaluated on the soil moisture pulse DOY for each station-year. For all SNOTEL stations, the median number of PDD on the soil moisture pulse DOY was 81 (mean = 67 PDD, ± 55 PDD), and the median density was 355 kg m^{-3} (mean = 364 kg m^{-3}, ± 73 kg m^{-3}). The median number of PDD on soil moisture pulse DOY decreased as elevation increased, with a median of 170 PDD at the lowest elevation (1,000–1,250 m) SNOTEL stations and a median of 20 PDD at the highest elevation (3,500–3,750 m) SNOTEL stations (Figure 16c). The PDD number on soil moisture pulse dates increased to the west and to the north (Figure 16a-b). Snow density on soil moisture pulse dates followed a similar pattern, with higher elevation SNOTEL stations seeing lower median densities (319 kg m^{-3}) than low elevation SNOTEL sites (444 kg m^{-3}). Median densities similarly increased to the west and north (Figure 17a-b). Stations in the northernmost latitude (48–49°) had a median density of 466 kg m^{-3}, while those in southernmost latitude (35–36°) had a median density of 319 kg m^{-3}. Stations in easternmost longitude (-105°; continental climate) had a median density of 316 kg m^{-3}, while stations located in the westernmost longitude (-123°; maritime climate) had a median density of 437 kg m^{-3}. SNOTEL stations within the maritime snow class exhibited the highest median PDD (Figure 16d) and densities (Figure 17d) with 135 and 480 kg m^{-3}, respectively. Prairie (364 kg m^{-3}, 65 PDD), montane forest (349 kg m^{-3}, 67 PDD), boreal forest (341 kg m^{-3}, 46 PDD), and tundra (314 kg m^{-3}, 23 PDD) snow classes had lower median densities and PDD on soil moisture pulse DOY.

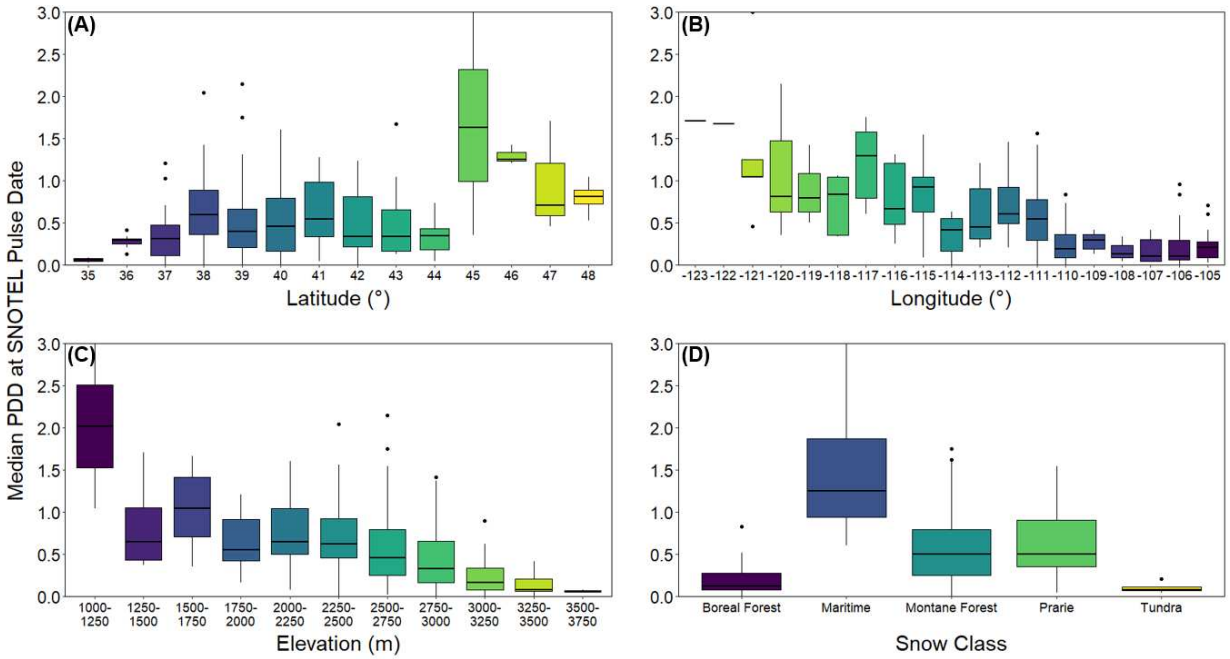

Figure 16: Median PDD on SNOTEL soil moisture pulse DOY by A) latitude, B) longitude, C) elevation, D) snow class.

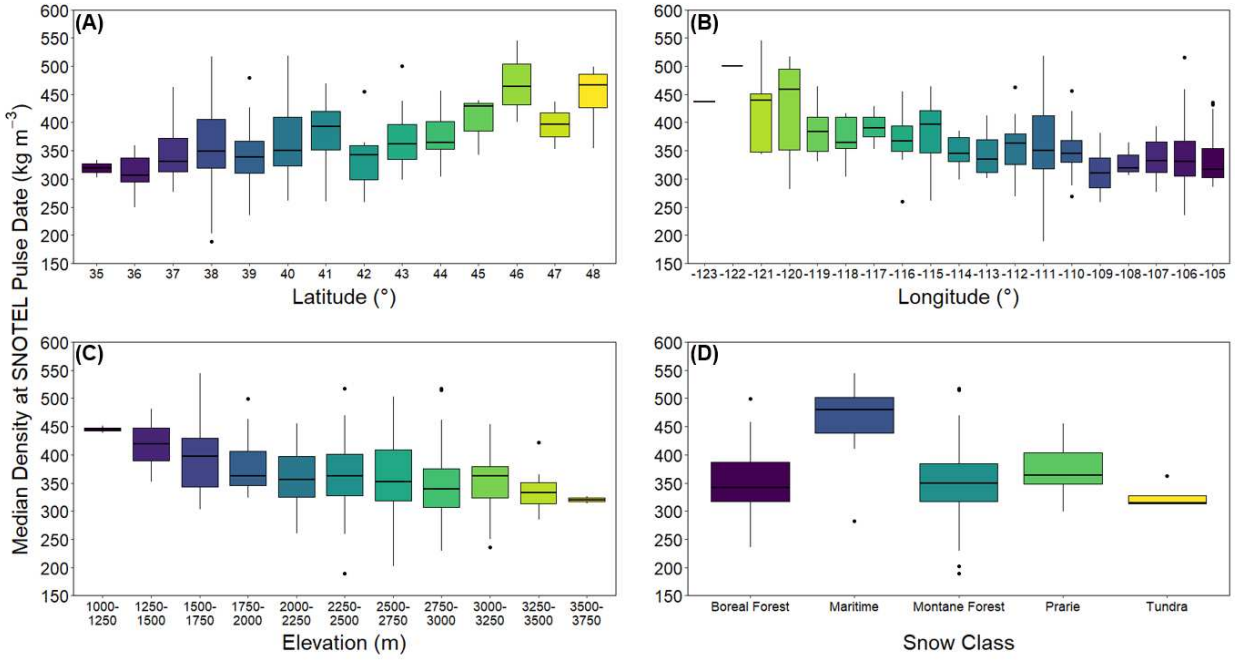

Figure 17: Median density (kg m^{-3}) on SNOTEL soil moisture pulse DOY by A) latitude, B) longitude, C) elevation, D) snow class.

3.3 Sentinel-1 SAR-Derived Estimates of Snowmelt Runoff Onset

Sentinel-1 SAR snowmelt runoff onset occurred an average of 0.76 ± 25.3 days and a median of 3 days after SNOTEL soil moisture pulses (Figure 18), which, to add context, improved from an average of 2.2 days with the original unfiltered data (Figure 19). The range of median temporal offset between Sentinel-1 SAR melt output and SNOTEL soil moisture pulses was within 3 days for SNOTEL stations at elevations between 1,250–3,000 m, whereas higher elevation (3,000–3,750 m) and the lowest elevation (1,000–1,250 m) stations exhibited an overall range in median temporal offset of 7–20 days, and 8 days, respectively (Figure 20).

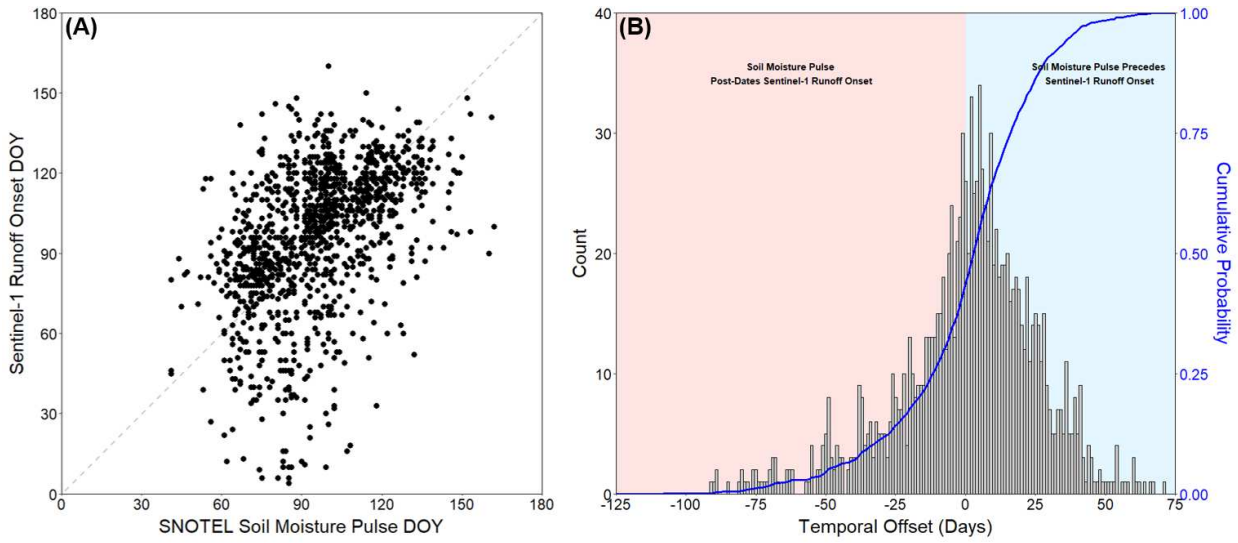

Figure 18: A) Scatterplot showing the relationship between Sentinel-1 SAR estimate of snowmelt runoff onset DOY and SNOTEL soil moisture pulse DOY (R^2 = 0.2, RMSE = 18.4 days), and B) histogram of the temporal offset (days) between Sentinel-1 SAR estimate of snowmelt runoff onset DOY and soil moisture pulse DOY, with corresponding cumulative probability curve (blue). Negative values (shaded in red) indicate soil moisture pulse DOY post-dates Sentinel-1 SAR estimate of snowmelt runoff onset DOY, while positive values (shaded in blue) indicate soil moisture pulse DOY precedes Sentinel-1 SAR estimate of snowmelt runoff onset DOY.

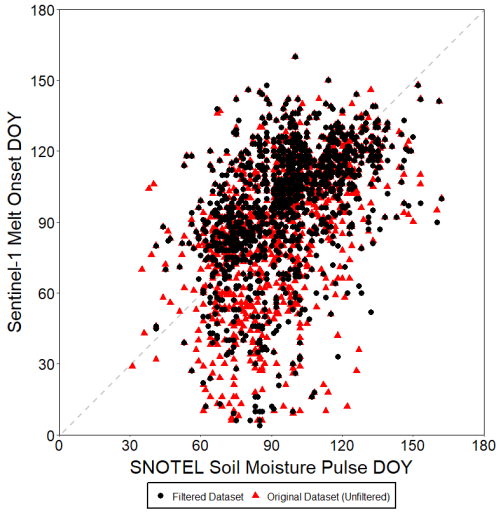

Figure 19: Sentinel-1 snowmelt runoff onset DOY plotted against SNOTEL soil moisture pulse DOY, showing the difference between the original, unfiltered dataset (red) and the filtered dataset (black). Temporal offset between SNOTEL soil moisture pulses and Sentinel-1 SAR estimates of snowmelt runoff onset improved from an average of -2.2 (median = 2, standard deviation = 26.1) with the original unfiltered data, to an average of 0.76 (median = 3, standard deviation = 25.29) with the filtered dataset.

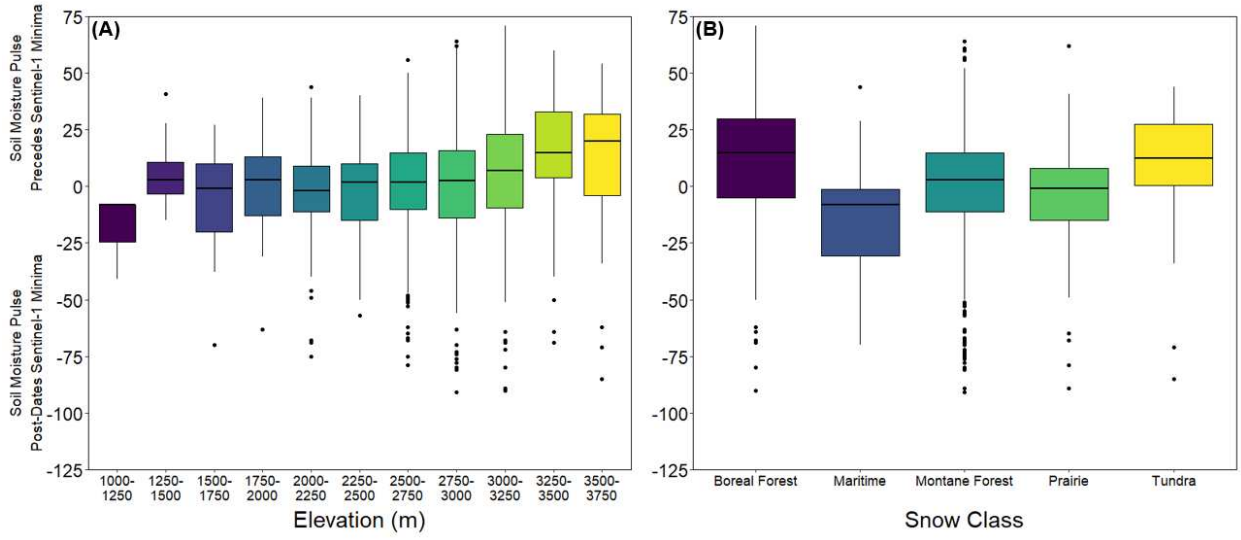

Figure 20: Temporal offset between Sentinel-1 SAR estimates of snowmelt runoff onset DOY and SNOTEL soil moisture pulse DOY, binned by A) elevation and B) snow class. Temporal offset was calculated by subtracting SNOTEL soil moisture pulse DOY from Sentinel-1 SAR estimates of snowmelt runoff onset DOY, negative values indicate Sentinel-1 SAR estimate of snowmelt runoff onset DOY precedes SNOTEL soil moisture pulse DOY, while positive values

indicate SNOTEL soil moisture pulse DOY precedes Sentinel-1 SAR estimate of snowmelt runoff onset DOY.

For elevations between 2,250–3,750 m, SNOTEL soil moisture pulses preceded Sentinel-1 SAR snowmelt runoff onset. SNOTEL stations between 1,250–2,250 m varied in reporting SNOTEL soil moisture pulses preceding and post-dating Sentinel-1 SAR snowmelt runoff onset, but the total range of median temporal offset was within 1–3 days. Stations located at the lowest elevation (1,000–1,250 m) saw SNOTEL soil moisture pulses post-date Sentinel-1 SAR snowmelt runoff onset. In comparing the offset between ascending (evening) and descending passes (morning), in 34% of cases ascending passes occurred first, whereas in 31% of cases descending passes occurred first (no available comparison for remaining 35%). I did not observe any significant differences in snowmelt runoff onset timing between the descending and ascending Sentinel-1 overpasses (Figure 21).

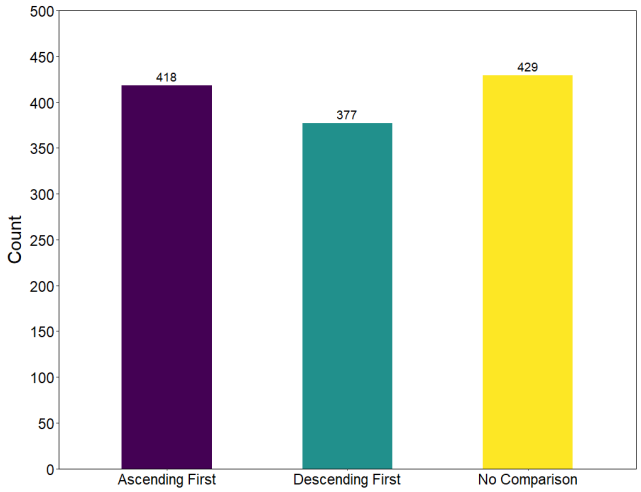

Figure 21: No significant diurnal differences in snowmelt runoff onset timing between descending and ascending passes were observed.

In comparison to peak SWE DOY, Sentinel-1 SAR snowmelt runoff onset occurred an average of 1.5 ± 24.1 days and a median of 6 days later (Figure 22). All elevation bins with the exception of 1,000–1,250 m reported SNOTEL peak SWE DOY preceding Sentinel-1 SAR snowmelt runoff onset DOY. The overall range of median temporal offset between Sentinel-1 SAR melt output and SNOTEL peak SWE for elevations between 1,500–2,750 m and 3,500–3,750 m was within 7 days. SNOTEL stations within elevation bin 1,000–1,250 m had a median temporal offset of 21 days, reporting SNOTEL peak SWE DOY post-dating Sentinel-1 SAR snowmelt runoff onset DOY, while elevation bin 1,250–1,500 m reported a median temporal offset of 14 days with SNOTEL peak SWE DOY preceding Sentinel-1 SAR snowmelt runoff onset DOY. SNOTEL stations at higher elevations (2,750–3,500 m) had a median temporal offset of 8–11 days.

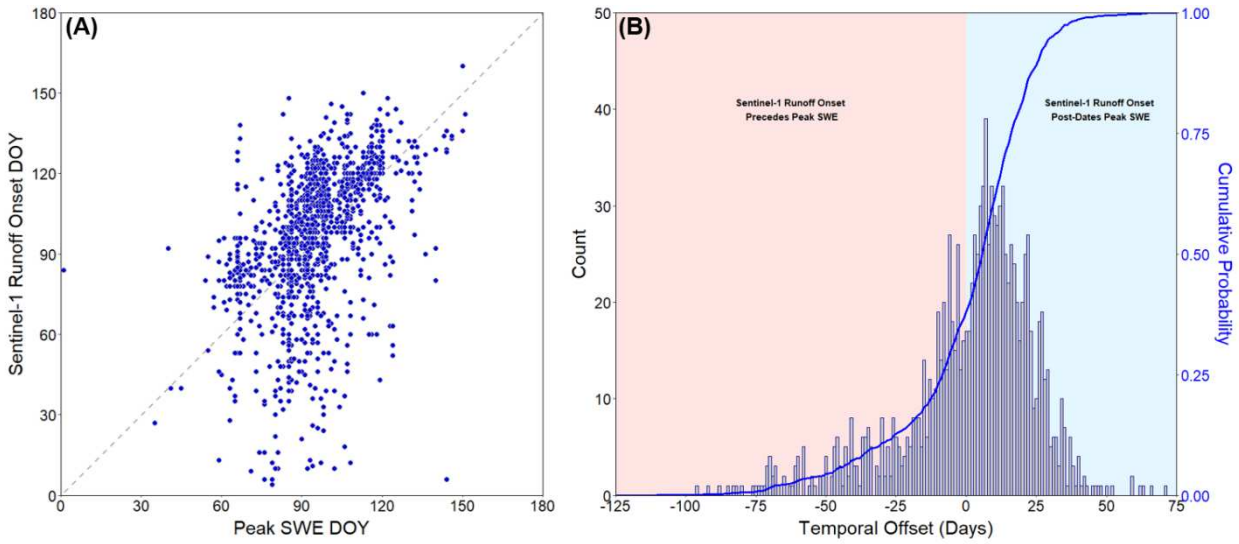

Figure 22: Paired A) scatterplot showing the relationship between Sentinel-1 SAR estimate of snowmelt runoff onset DOY and SNOTEL peak SWE DOY (R^2 = 0.2, RMSE = 14.9 days), and B) histogram of the temporal offset (days) between Sentinel-1 SAR estimate of snowmelt runoff onset DOY and SNOTEL peak SWE DOY, with corresponding cumulative probability curve (blue). Negative values (shaded in red) indicate SNOTEL peak SWE DOY post-dates Sentinel-1 SAR estimate of snowmelt runoff onset DOY, while positive values (shaded in blue) indicate SNOTEL peak SWE DOY precedes Sentinel-1 SAR estimate of snowmelt runoff onset DOY.

4. DISCUSSION

4.1 Uncertainty, Limitations of Analyses

4.1.1 Differences in Spatial Scales

This study evaluates and compares snowmelt runoff onset at two different spatial scales. SNOTEL station-derived snowmelt runoff onset via soil moisture pulse is at the point scale, while Sentinel-1 SAR estimates of snowmelt runoff onset are averaged over a 1 km^2 area of representative pixels to improve the strength of the snow signal. However, the coarseness of the 1 km^2 area smooths small-scale effects that local topography may have on melt progression, which act on the snowpack in the vicinity of the SNOTEL station that contributes to melt output picked up by the soil moisture sensor. A similar approach is used by Lievens et al. (2019) to improve the accuracy of snow depths derived from Sentinel-1. The progression of snowmelt in complex mountainous terrain is not homogeneous, as various topographic controls on melt distribution, like solar radiation (Cline, 1997; Marks & Dozier, 1992) and spring intra-snowpack meltwater flow (Webb et al., 2022) are associated with high degrees of spatial variability. While point measurements have been used in the past to estimate the spatial distribution of SWE over larger areas (Harshburger et al., 2010; Jörg-Hess et al., 2014), it is important to mention that studies have observed significant variability in measurements of SWE and snow depth from the point to area scale in the vicinity surrounding SNOTEL stations (Meromy et al., 2013; Molotch & Bales, 2005). SNOTEL stations tend to be located in small meadows within flat, forested areas, which often fail to fully represent the broader heterogeneity of complex topography in mountainous regions, and biases should be considered when using these stations for validation (Gleason et al., 2017).

4.1.2 Sentinel-1 SAR Orbital Repeat Period

The Sentinel-1 mission originally was planned as a two-satellite constellation. Sentinel-1A launched in April 2014 and provided 12-day orbital repeat coverage until the launch of Sentinel-1B in April 2016, when the orbital repeat period reduced to 6-days. After the decommissioning of Sentinel-1B in August of 2022 after a power issue experienced in December of 2021, only Sentinel-1A remained operational. As a result, the orbital repeat period increased to approximately 12 days from the same orbital plane for imagery after December 2021, decreasing the number of total observations throughout the melt season. Coarsening the temporal resolution to almost two weeks between image acquisitions adds substantial temporal uncertainty. The increase in soil moisture that is associated with melt output from the snowpack and detected by the SNOTEL soil moisture pulse occurs rapidly for most sites and could be missed with a 12-day orbital repeat period, with the fastest pulses occurring during a single day, although this output is the culmination of snowpack moistening and ripening that occurs over a period of days to weeks. Currently, most automated stations do not include LWC nor snow temperature observations, but both of these would provide valuable information on snowpack evolution leading up to SNOTEL and Sentinel-1 observations of melt output.

4.2 Context Within the Western U.S.

4.2.1 Quality of SNOTEL Soil Moisture Pulse

By nature of the measurement approach, the SNOTEL soil moisture observation captures the start of the runoff phase, where water is released from the snowpack and into the subsurface.

While the pulse indicates the beginning of melt output, it is a snapshot of the endmember state of the snowpack and cannot characterize or measure the length of the ripening or runoff phases. Preferential flow paths can also develop throughout the snowpack and result in the high spatial variability of distribution of liquid water, which could impact the timing and location of melt output (Webb et al., 2018, 2022), in addition to the quality of the soil moisture pulse.

Snowpacks in continental zones had the highest percentages of Grade 1 pulses, with Colorado reporting the highest percentage of Grade 1 pulses (74%), along with Wyoming (56%). These snowpacks are characterized as cold and dry prior to melt onset (Mock & Birkeland, 2000; Trujillo & Molotch, 2014), which is conducive to producing a distinct pulse corresponding to a sharp increase in soil moisture as liquid water leaves the snowpack. While Grade 1 pulses were found across all elevations except for the lowest (1,000–1,250 m), they accounted for the vast majority of pulses in high elevation (2,750–3,750 m) sites, which commonly correspond to continental snow regimes (Trujillo & Molotch, 2014).

Conversely, while Grade 2 and Grade 3 pulses were found across all elevations, both were found in greater numbers at lower elevations (1,000–1,500 m). Grade 2 pulses, characterized by a more gradual pulse, often associated with a smaller magnitude pulse occurring prior to a larger magnitude pulse, were well-distributed throughout the intermountain and maritime snow zones. Intermountain snowpacks are typically shallower than those in maritime regions and deeper than continental snowpacks, and experience warmer climates than continental snowpacks, but are colder in climate compared to maritime regions (Evan & Eisenman, 2021; Trujillo & Molotch, 2014). Snowpacks in the maritime zone (California, Oregon, Washington) had the highest percentages of Grade 3 pulses (44%), which are characterized by little to no fluctuation or discernable increase in the soil moisture timeseries throughout the melt season.

Maritime regions experience warmer temperatures and greater precipitation (Gray & Male, 1981; Trujillo & Molotch, 2014; Sturm et al., 1995), commonly undergo mid-winter melt (Nolin & Daly, 2006; Sproles et al., 2013), and lack cold content compared to colder, drier regions (Jennings et al., 2018). Drier snowpacks in continental regions remain below 0 °C throughout the winter and early spring and are too cold to contain liquid water, whereas snowpacks in intermountain and maritime regimes that are warmer and remain close to isothermal for a longer period of time during the melt season can be wet and intermittently output liquid water (Jennings et al., 2018; Katz et al., 2023), thus diminishing the clarity of soil moisture pulse signal. As a result of intermittent water output into the soil, soil moisture conditions do not exhibit a comparably sharp increase indicative of the beginning of the runoff phase, resulting in a Grade 3 pulse.

4.2.2 Timing of SNOTEL Soil Moisture Pulse

Soil moisture pulse dates occur latest in snowpacks classified as maritime, which tend to accumulate deep (>300 cm SWE) and dense snowpacks (Sturm & Liston, 2021; Trujillo & Molotch, 2014), but do not show strong trends related to elevation, suggesting that local climatology, terrain features, and vegetation structure have a stronger influence on snowmelt runoff onset. Soil moisture pulses occur earliest in montane forest and prairie snowpacks. In montane forests, canopy cover and structure combined with intermittent periods of melt and refreezing throughout the spring dictate snow distribution and melt (Bonner et al., 2022), whereas snowpacks in prairie environments are susceptible to wind redistribution and snow cover is more ephemeral (Sturm & Liston, 2021; Webb et al., 2020). In relation to peak SWE, we found that SNOTEL soil moisture pulses on average post-dated peak SWE (Figure 5). On

average, soil moisture pulses occur at an average of 88% of peak SWE, which is fairly consistent across latitudes, longitudes, elevations, and snow classes, though the timing of peak SWE differs across latitudes, longitudes, elevations, and snow classes (Figure 23).

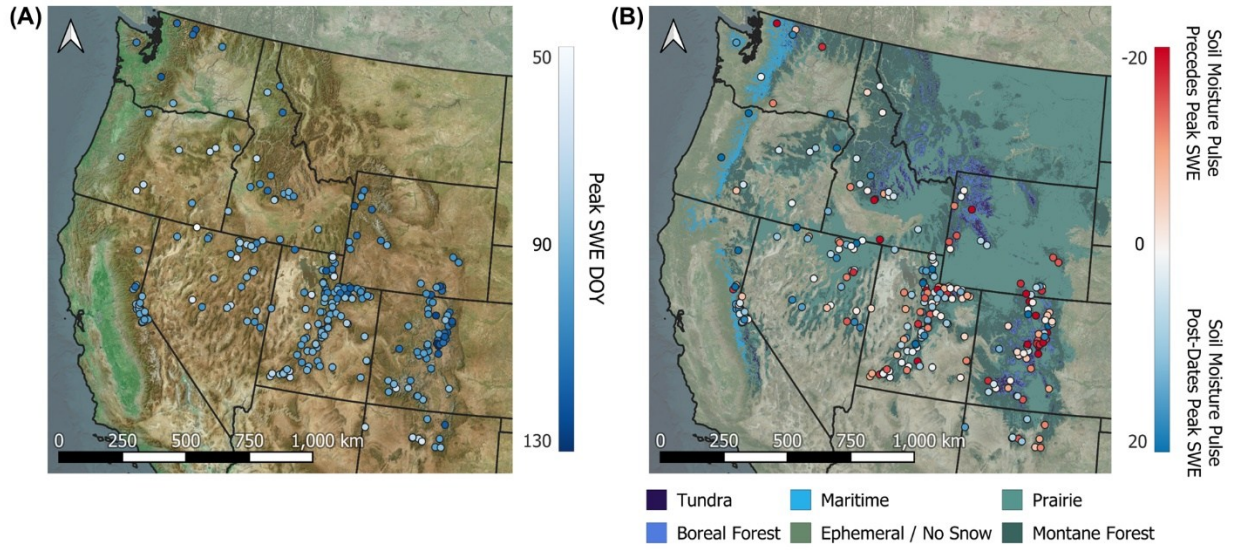

Figure 23: Locations of 260 SNOTEL stations across the western U.S. with points colored by A) median peak SWE DOY, and B) the difference (days) between the median soil moisture pulse DOY and peak SWE DOY. Negative difference (days) indicates the soil moisture pulse precedes peak SWE, while positive difference (days) indicates the soil moisture pulse post-dates peak SWE. Snow classifications (Sturm & Liston, 2021) are also shown in panel B).

Assessing climatological conditions in which SNOTEL soil moisture pulses occur across the western U.S. provides an important frame of reference for conditions that corroborate snowmelt runoff onset in varying terrain. We found that both median PDD and densities on SNOTEL soil moisture pulse DOY increased to the west and north. Similarly, maritime snowpacks experienced the most cumulative PDD and highest median densities on the soil moisture pulse DOY. The deeper maritime snowpacks, found in the mountains California and the Pacific Northwest, are products of a wet and relatively warmer and higher humidity climate (Sturm & Liston, 2021; Trujillo & Molotch, 2014) than intermountain and continental regions

and experiences increased and faster rates of compaction and densification (Sturm & Holmgren, 1998).

Both median PDD and densities decreased with increasing elevation, showing that snow at high elevations is less dense and experiences fewer warm days when it begins to output melt than snow at lower elevations, where temperatures are colder relative to low elevations (Wetlaufer et al., 2016) and precipitation mainly occurs as snow (Biggs & Whitaker, 2012; Yu et al., 2024). Snowpacks in the southern Rocky Mountains were less dense than their northwestern maritime counterparts, and experienced fewer cumulative PDD on the soil moisture pulse DOY. As the distance from Pacific sources of moisture increases, the snowpack becomes colder, drier, and shallower (Mock & Birkeland, 2000), corresponding with lower density snow than maritime regions. Boreal forest and tundra snowpacks reported the lowest median densities and fewest PDD at higher elevations. Boreal forest and tundra snow typically exist in environments that are cold enough to produce stratigraphy with low-density facets and depth hoar that comprise a larger proportion of the snowpack (Sturm & Liston, 2021; Zhao et al., 2023), and experience slower densification than snowpacks located in warmer and wetter climates (Mizukami & Perica, 2008; Sturm & Holmgren, 1998).

4.2.3 Timing of Sentinel-1 SAR Estimates of Snowmelt Runoff Onset

Sentinel-1 estimates of snowmelt runoff onset occurred earliest in snowpacks classified as maritime and at lower elevations (1,000–1,250 m). This makes sense, as maritime climates are warmer and wetter than those in intermountain regions (Gray & Male, 1981; Trujillo & Molotch, 2014; Sturm et al., 1995), and warmer temperatures (Hunsaker et al., 2012; Mote et al., 2005;

Musselman et al., 2017) and rain-on-snow events (Juras et al., 2021; Morán-Tejeda et al., 2016) are more common at lower elevations. Sentinel-1 estimates of snowmelt runoff onset occurred latest in snowpacks classified as boreal forest and tundra, where forest canopy structure (Metcalfe & Buttle, 1998; Roth & Nolin, 2017; Webb et al., 2020) and wind transport and landscape features (Benson & Sturm, 1993; Liston & Sturm, 2002; Pomeroy et al., 2006) dictate snow distribution and melt processes, respectively, and at high elevations with colder temperatures and precipitation mainly occurring in the form of snow (Biggs & Whitaker, 2012; Gagliano et al., 2023; Yu et al., 2024).

SNOTEL stations between 1,250–3,000 m and within montane forest and prairie snow classes reported the lowest temporal offset (median = 3 days) between Sentinel-1 SAR estimates of snowmelt runoff onset and SNOTEL soil moisture pulses, which is in part due to the increased occurrence of Grade 1 pulses. We found that 68% of Grade 1 pulses occur in montane forests and 10% occur in the prairie class. Grade 1 pulses account for 52% of total pulses within the montane forest snow class, and 60% of the prairie snow class. In these environments, Sentinel-1 SAR does a fairly good job of detecting snowmelt runoff onset that has a closely associated, distinct physical signal. In locations with a greater temporal offset between SNOTEL soil moisture pulses and Sentinel-1 SAR estimates snowmelt runoff onset, automated station networks and day-of and hour-of records of SWE, air temperature, and density can help monitor melt progression and output, providing context to late or early signals of melt from spaceborne platforms (Lund et al., 2022).

4.2.4 Sensitivity of Snowmelt Runoff Onset Signals to Local Climatology

We found that SNOTEL soil moisture pulse signal quality and timing is sensitive to both local and regional climatologies. Stations located in drier and colder regimes produced a clearer and higher quality soil moisture pulse (e.g., Grade 1 pulses), while soil moisture pulses are often less distinct in wetter and warmer snow regimes. In the case of Sentinel-1 SAR, when the backscatter minimum is reached, the snow is saturated and the signal attenuates (Marin et al., 2020), meaning that snowmelt onset and runoff begin. Shallower snowpacks are more sensitive to diurnal changes in temperature relative to deeper snowpacks (Burns et al., 2014). Our findings were consistent with this, as we saw that deeper snowpacks with higher peak SWE often correlated with more stable backscatter timeseries and more distinct backscatter minima.

As an illustration of this interannual variability in SWE and soil moisture pulse, we show an example from the Monitor Pass SNOTEL station (CA_633, elevation = 2,533 m) for a low snow year (2015; 30% of median peak SWE) and a high snow year (2019; 176% of median peak SWE; Figure 24). The low snow year (Figure 24a) has a backscatter timeseries with limited variability and no clear minima, while the high snow year (Figure 24b) exhibits multiple orbits that each show a clear backscatter decrease before reaching a minimum and subsequently increasing again as runoff begins and SWE decreases.

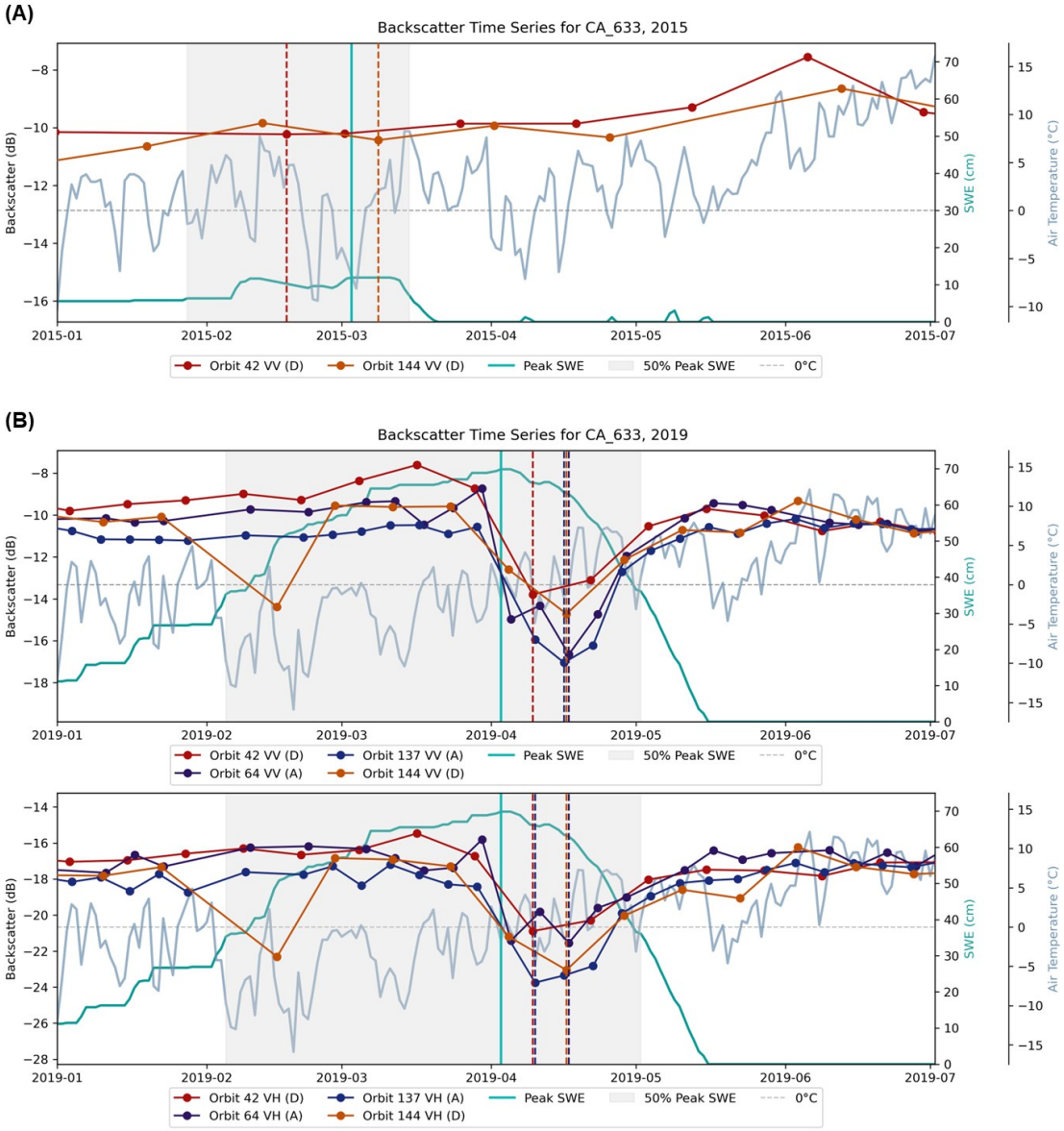

Figure 24: Backscatter timeseries for Monitor Pass SNOTEL station (CA_633) showing A) a low snow year in 2015 versus B) a high snow year in 2019. Top panels for both A) and B) show VV timeseries, while bottom panels show VH timeseries. There were no available VH acquisitions for snow year 2015. The grey dotted horizontal line shows SNOTEL air temperature at 0 °C. 50% peak SWE represents the period for potential melt output as the period between the first and last instance of 50% peak SWE.

4.3 Implications for the Remote Sensing of SWE Using Radar-Based Methods

4.3.1 Using In-Situ Snowpack Metrics to Inform L-Band SWE Retrievals

With the launch of NISAR in 2025, global L-band (1.25 GHz) radar coverage will be available at a 12-day repeat interval. L-band InSAR SWE-change retrievals are sensitive to the presence of LWC in the snowpack, which slows radar wave velocity given the high dielectric permittivity of water relative to dry snow and ice (Bradford et al., 2009) and can lead to uncertain estimates of SWE (Bonnell et al., 2021; Roy et al., 2017; Schwank & Naderpour, 2018). It is important to note that despite spatial and temporal challenges, methods for evaluating snowpack conditions do not operate in isolation – the fusion of a variety of methodologies is essential to facilitate a greater understanding of snowpack conditions and evolution throughout the melt season. Automated stations provide point observations with a wide variety of metrics that can be used to inform conditions that corroborate snowmelt development. However, most automated stations are not equipped to measure LWC or snow temperature, and more work is required to obtain a better understanding of LWC magnitudes and spatial variability throughout the melt season via detailed field observations. While the spatial footprint of Sentinel-1 SAR is comparatively large, backscatter thresholding approaches can help identify LWC presence in the snowpack (Lund et al., 2022; Nagler et al., 2016) on a spatial scale more relevant to NISAR snow hydrology applications. Despite the lack of sensitivity of the SNOTEL soil moisture pulse and Sentinel-1 SAR backscatter minima methodologies to the earlier moistening and ripening phases, we know that once melt output begins and the snowpack becomes saturated, L-band retrievals of SWE will not be accurate. Thus, the onset of the runoff phase can be used as a spatial and temporal mask for future NISAR SWE retrievals.

4.3.2 L-Band Sensitivity to Local Climatology

Understanding the climatological regime of the region being studied by consulting existing multi-year records from automated station networks and field observations of air temperature, PDD, density, creates a basis for how the snowpack may behave at different points throughout the accumulation and melt season. The 12-day repeat interval of NISAR matches the current temporal resolution of Sentinel-1, meaning that NISAR retrievals could be subject to similar uncertainties and challenges surrounding spatial and temporal resolution, and local and regional climatological sensitivity. A NISAR-derived estimate of snowmelt runoff onset using the backscatter minima methodology would likely be feasible, as signal attenuation by liquid water is dependent on signal frequency (Bradford et al., 2009), which points to L-band having better penetration in wet snow conditions than C-band, as the C-band wavelength is more sensitive to the formation of ice lenses and melt-freeze crusts (Brangers et al., 2024; Ruiz et al., 2022). Findings in this study demonstrate that we cannot necessarily assume a snowpack as dry or wet depending on the timing of the backscatter minima, SNOTEL soil moisture pulse, or peak SWE. To do so would ignore complex and dynamic melt processes and metamorphism that can occur within short periods of time in environments of complex terrain and at varying elevations (Colbeck, 1982; Laska et al., 2016).

5. FUTURE WORK

Given the trajectory of warming trends and projected changes in snowmelt timing and decrease in snowpack storage, the ability to accurately quantify SWE at high spatiotemporal scales across the globe is critical. Directly building off of the Sentinel-1 SAR backscatter minima approach for detecting snowmelt runoff onset presented in this thesis would be using backscatter change detection/thresholding methodologies to identify the presence of LWC in superficial layers of the snowpack (Lund et al., 2022; Manickam & Barros, 2020; Nagler et al., 2016). L-band SWE retrievals are challenged by the presence of LWC in the snowpack, which can occur before the runoff phase begins. Pairing snowmelt runoff estimates with estimates of surface layer melt via backscatter change detection/thresholding approaches would allow for the creation of a temporal window of uncertainty regarding L-band SWE retrievals, where runoff onset would indicate low accuracy in SWE retrievals and surface melt events would indicate periods of uncertainty in SWE retrievals.

The field campaign conducted throughout the 2024 melt season in Summit County, Colorado at multiple SNOTEL stations with varying elevations and topographical characteristics allows for paired analyses with automated stations and Sentinel-1 SAR estimates of snowmelt runoff onset that are novel and exciting. Repeated field campaigns in future years following a similar methodology would allow for a more robust comparison between estimates of runoff onset and snowpack evolution derived from automated stations and spaceborne platforms. Including automated stations located within different regions of the western U.S., like maritime or intermountain regions, that experience markedly different climatic conditions during the melt season than colder and drier Colorado snowpacks would make this comparison richer and lead to a broader understanding of snowpack evolution across varying climatic regimes and

climatological conditions. Additionally, adapting existing automated station networks to include snowpack temperature and LWC sensors would enable a more accurate and detailed assessment of melt progression throughout the season and more closely simulate the measurements collected manually in snowpits during field surveys, as SNOTEL soil moisture sensors alone do not provide metrics of intra-snowpack melt processes. The U.S. Geological Survey (USGS) has made significant progress in deploying a new, updated network of meteorological stations called the Next Generation Water Observing System (NGWOS) across the western U.S., which currently consists of 14 stations distributed throughout the Upper Colorado River Basin (U.S. Geological Survey, 2021). The NGWOS stations will include additional metrics, including snow temperature and LWC, and presents an exciting opportunity for future analyses once the network becomes fully operational.

6. CONCLUSION

In this study, I integrated field measurements, 260 automated stations, and Sentinel-1 SAR estimates of snowmelt runoff onset to assess how snowpack characteristics evolve prior to and after Sentinel-1 SAR-derived snowmelt runoff onset. I developed an algorithm to detect the observed rapid increase in soil moisture, defined as the "pulse", associated with meltwater output from the snowpack to the ground surface to serve as a proxy for snowmelt runoff onset at SNOTEL stations.

This research demonstrates that snowmelt runoff onset detected via SNOTEL soil moisture pulses post-dates peak SWE by a median of 3 days (± 18.2 days) and occur at 88% (median 92%, ± 13%) of peak SWE on average, which remains consistent across all sampled latitudes, longitudes, and elevations. When considering the different snow classes, tundra snow class pulses occurred at a median 94% peak SWE, boreal forest, montane forest, and prairie pulses occurred at a median 92% peak SWE, and maritime pulses occurred at a median 89% peak SWE. SNOTEL densities and number of PDD on soil moisture pulse dates increased with latitude and longitude and decreased with elevation. Soil moisture pulse dates occurred latest in maritime snowpacks, characterized by short accumulation seasons resulting in large accumulations of dense snow (Sturm & Liston, 2021; Trujillo & Molotch, 2014) and earliest in montane forest/prairie snowpacks, where snow distribution and melt are dictated by canopy cover combined with intermittent periods of melt and refreezing throughout the spring, and wind distribution and less stable snow cover, respectively.

Through comparing 260 paired SNOTEL soil moisture pulses and Sentinel-1 SAR estimates of snowmelt runoff onset, I found that SNOTEL soil moisture pulses preceded Sentinel-1 SAR estimates of snowmelt runoff onset by a median 3 days (± 25.3 days). Sentinel-1

estimates of snowmelt runoff onset occurred earliest in snowpacks classified as maritime and at lower elevations and latest in snowpacks classified as boreal forest and tundra. SNOTEL stations between 1,250–3,000 m and within montane forest and prairie snow classes reported the lowest temporal offset (median = 3 days) between Sentinel-1 SAR estimates of snowmelt runoff onset and SNOTEL soil moisture pulses. Montane forest and prairie snowpacks both had majority Grade 1 pulses, likely contributing to the low temporal offset. In locations with a greater temporal offset between SNOTEL soil moisture pulses and Sentinel-1 SAR estimates, automated station networks and day-of and hour-of records of SWE, air temperature, and density can help monitor melt progression and output, providing context to late or early signals of melt from spaceborne platforms.

For both Sentinel-1 SAR-derived estimates of snowmelt runoff onset and SNOTEL soil moisture pulses, I found that local climatological conditions had a strong impact on snowmelt runoff onset signal quality and timing. The progression of snowmelt in complex mountainous terrain is not homogeneous, as various topographic controls on melt distribution, like solar radiation (Cline, 1997; Marks & Dozier, 1992) and spring intra-snowpack meltwater flow (Webb et al., 2022) are associated with high degrees of spatial variability. The accuracy of InSAR SWE retrievals is highly sensitive to the presence of liquid water, given its high dielectric permittivity compared to dry snow, and with the upcoming launch of NISAR, continued research focused on snowpack evolution, specifically LWC development and spatial variability, throughout the melt season will be required to improve the accuracy of radar-based SWE retrievals. By analyzing snowpack conditions leading up to the runoff phase and comparing snowmelt runoff onset estimates from SNOTEL stations and Sentinel-1 SAR, my research provides important insights into the variability in the progression of snowmelt and timing of the runoff phase across different

climatic regimes in the western U.S., which can be used to improve future NISAR SWE retrievals. Improving the accuracy of spaceborne SWE retrievals will allow water managers to make more informed decisions regarding water resource management given the trajectory of warming trends and projected changes in snowmelt timing and decrease in snowpack storage.

REFERENCES

Awasthi, S., & Varade, D. (2021). Recent advances in the remote sensing of alpine snow: A review. GIScience & Remote Sensing, 58(6), 852–888. https://doi.org/10.1080/15481603.2021.1946938

Barnett, T. P., Adam, J. C., & Lettenmaier, D. P. (2005). Potential impacts of a warming climate on water availability in snow-dominated regions. Nature, 438(7066), 303–309. https://doi.org/10.1038/nature04141

Barry, R. G., & Gan, T. Y. (2022). The Global Cryosphere: Past, Present, and Future. Cambridge University Press.

Benson, C. S., & Sturm, M. (1993). Structure and wind transport of seasonal snow on the Arctic slope of Alaska. Annals of Glaciology, 18, 261–267. https://doi.org/10.3189/S0260305500011629

Berghuijs, W. R., Woods, R. A., & Hrachowitz, M. (2014). A precipitation shift from snow towards rain leads to a decrease in streamflow. Nature Climate Change, 4(7), 583–586. https://doi.org/10.1038/nclimate2246

Biggs, T. W., & Whitaker, T. M. (2012). Critical elevation zones of snowmelt during peak discharges in a mountain river basin. Journal of Hydrology, 438–439, 52–65. https://doi.org/10.1016/j.jhydrol.2012.02.048

Blankinship, J. C., Meadows, M. W., Lucas, R. G., & Hart, S. C. (2014). Snowmelt timing alters shallow but not deep soil moisture in the Sierra Nevada. Water Resources Research, 50(2), 1448–1456. https://doi.org/10.1002/2013WR014541

Bonnell, R., Elder, K., McGrath, D., Marshall, H. P., Starr, B., Adebisi, N., Palomaki, R. T., & Hoppinen, Z. (2024). L-Band InSAR Snow Water Equivalent Retrieval Uncertainty Increases With Forest Cover Fraction. Geophysical Research Letters, 51(24), e2024GL111708. https://doi.org/10.1029/2024GL111708

Bonnell, R., McGrath, D., Williams, K., Webb, R., Fassnacht, S. R., & Marshall, H.-P. (2021). Spatiotemporal Variations in Liquid Water Content in a Seasonal Snowpack: Implications for Radar Remote Sensing. Remote Sensing, 13(21), 4223. https://doi.org/10.3390/rs13214223

Bonner, H. M., Raleigh, M. S., & Small, E. E. (2022). Isolating forest process effects on modelled snowpack density and snow water equivalent. Hydrological Processes, 36(1), e14475. https://doi.org/10.1002/hyp.14475

Bradford, J. H., Harper, J. T., & Brown, J. (2009). Complex dielectric permittivity measurements from ground-penetrating radar data to estimate snow liquid water content in the pendular regime. Water Resources Research, 45(8), 2008WR007341. https://doi.org/10.1029/2008WR007341

Brangers, I., Marshall, H.-P., De Lannoy, G., Dunmire, D., Mätzler, C., & Lievens, H. (2024). Tower-based C-band radar measurements of an alpine snowpack. The Cryosphere, 18(7), 3177–3193. https://doi.org/10.5194/tc-18-3177-2024

Broxton, P. D., Dawson, N., & Zeng, X. (2016). Linking snowfall and snow accumulation to generate spatial maps of SWE and snow depth. Earth and Space Science, 3(6), 246–256. https://doi.org/10.1002/2016EA000174

Burns, S. P., Molotch, N. P., Williams, M. W., Knowles, J. F., Seok, B., Monson, R. K., Turnipseed, A. A., & Blanken, P. D. (2014). Snow Temperature Changes within a Seasonal Snowpack and Their Relationship to Turbulent Fluxes of Sensible and Latent Heat. Journal of Hydrometeorology, 15(1), 117–142. https://doi.org/10.1175/JHM-D-13-026.1

Campbell, J. L., Mitchell, M. J., Groffman, P. M., Christenson, L. M., & Hardy, J. P. (2005). Winter in northeastern North America: A critical period for ecological processes. Frontiers in Ecology and the Environment, 3(6), 314–322. https://doi.org/10.1890/1540-9295(2005)003[0314:WINNAA]2.0.CO;2

Carroll, T., Cline, D., Fall, G., Nilsson, A., Li, L., & Rost, A. (2001). NOHRSC operations and the simulation of snow cover properties for the coterminous US. Proc. 69th Annual Meeting of the Western Snow Conf.

Cayan, D. R., Dettinger, M. D., Kammerdiener, S. A., Caprio, J. M., & Peterson, D. H. (2001). Changes in the Onset of Spring in the Western United States. Bulletin of the American Meteorological Society, 82(3), 399–415. https://doi.org/10.1175/1520-0477(2001)082<0399:CITOOS>2.3.CO;2

Cline, D. W. (1997). Snow surface energy exchanges and snowmelt at a continental, midlatitude Alpine site. Water Resources Research, 33(4), 689–701. https://doi.org/10.1029/97WR00026

Clow, D. W. (2010). Changes in the Timing of Snowmelt and Streamflow in Colorado: A Response to Recent Warming. Journal of Climate, 23(9), 2293–2306. https://doi.org/10.1175/2009JCLI2951.1

Cohen, J., & Entekhabi, D. (2001). The influence of snow cover on northern hemisphere climate variability. Atmosphere-Ocean, 39(1), 35–53. https://doi.org/10.1080/07055900.2001.9649665

Colbeck, S. C. (1977). Short-Term Forecasting of Water Run-Off From Snow and Ice. Journal of Glaciology, 19(81), 571–588. https://doi.org/10.3189/S0022143000215487

Colbeck, S. C. (1982). An overview of seasonal snow metamorphism. Reviews of Geophysics, 20(1), 45–61. https://doi.org/10.1029/RG020i001p00045

Condon, L. E., Atchley, A. L., & Maxwell, R. M. (2020). Evapotranspiration depletes groundwater under warming over the contiguous United States. Nature Communications, 11(1), 873. https://doi.org/10.1038/s41467-020-14688-0

Darychuk, S. E., Shea, J. M., Menounos, B., Chesnokova, A., Jost, G., & Weber, F. (2023). Snowmelt characterization from optical and synthetic-aperture radar observations in the La Joie

Basin, British Columbia. The Cryosphere, 17(4), 1457–1473. https://doi.org/10.5194/tc-17-1457-2023

Deems, J. S., Painter, T. H., & Finnegan, D. C. (2013). Lidar measurement of snow depth: A review. Journal of Glaciology, 59(215), 467–479. https://doi.org/10.3189/2013JoG12J154

Déry, S. J., & Brown, R. D. (2007). Recent Northern Hemisphere snow cover extent trends and implications for the snow-albedo feedback. Geophysical Research Letters, 34(22), 2007GL031474. https://doi.org/10.1029/2007GL031474

Dingman, S. L. (2015). Physical Hydrology (3rd ed.). Waveland Press.

Diro, G. T., & Sushama, L. (2020). Contribution of Snow Cover Decline to Projected Warming Over North America. Geophysical Research Letters, 47(1), e2019GL084414. https://doi.org/10.1029/2019GL084414

Earman, S., Campbell, A. R., Phillips, F. M., & Newman, B. D. (2006). Isotopic exchange between snow and atmospheric water vapor: Estimation of the snowmelt component of groundwater recharge in the southwestern United States. Journal of Geophysical Research: Atmospheres, 111(D9), 2005JD006470. https://doi.org/10.1029/2005JD006470

Evan, A., & Eisenman, I. (2021). A mechanism for regional variations in snowpack melt under rising temperature. Nature Climate Change, 11(4), 326–330. https://doi.org/10.1038/s41558-021-00996-w

Fleming, S. W., Zukiewicz, L., Strobel, M. L., Hofman, H., & Goodbody, A. G. (2023). SNOTEL, the Soil Climate Analysis Network, and water supply forecasting at the Natural Resources Conservation Service: Past, present, and future. JAWRA Journal of the American Water Resources Association, 59(4), 585–599. https://doi.org/10.1111/1752-1688.13104

Foster, J. L., Sun, C., Walker, J. P., Kelly, R., Chang, A., Dong, J., & Powell, H. (2005). Quantifying the uncertainty in passive microwave snow water equivalent observations. Remote Sensing of Environment, 94(2), 187–203. https://doi.org/10.1016/j.rse.2004.09.012

Gagliano, E., Shean, D., Henderson, S., & Vanderwilt, S. (2023). Capturing the Onset of Mountain Snowmelt Runoff Using Satellite Synthetic Aperture Radar. Geophysical Research Letters, 50(21), e2023GL105303. https://doi.org/10.1029/2023GL105303

Gao, B., & Ma, W. (2024). Capturing Snowmelt Runoff Onset Date under Different Land Cover Types Using Synthetic Aperture Radar: Case Study of Sierra Nevada Mountains, USA. Applied Sciences, 14(15), 6844. https://doi.org/10.3390/app14156844

Garvelmann, J., Pohl, S., & Weiler, M. (2013). From observation to the quantification of snow processes with a time-lapse camera network. Hydrology and Earth System Sciences, 17(4), 1415–1429. https://doi.org/10.5194/hess-17-1415-2013

Gleason, K. E., Nolin, A. W., & Roth, T. R. (2017). Developing a representative snow-monitoring network in a forested mountain watershed. Hydrology and Earth System Sciences, 21(2), 1137–1147. https://doi.org/10.5194/hess-21-1137-2017

Gray, D. M., & Male, D. H. (Eds.). (1981). Handbook of snow (Vol. 776). Toronto, Canada: Pergamon Press.

Groisman, P. Ya., Karl, T. R., & Knight, R. W. (1994). Observed Impact of Snow Cover on the Heat Balance and the Rise of Continental Spring Temperatures. Science, 263(5144), 198–200. https://doi.org/10.1126/science.263.5144.198

Guan, B., Molotch, N. P., Waliser, D. E., Fetzer, E. J., & Neiman, P. J. (2010). Extreme snowfall events linked to atmospheric rivers and surface air temperature via satellite measurements. Geophysical Research Letters, 37(20), 2010GL044696. https://doi.org/10.1029/2010GL044696

Guneriussen, T., Hogda, K. A., Johnsen, H., & Lauknes, I. (2000). InSAR for estimation of changes in snow water equivalent of dry snow. IGARSS 2000. IEEE 2000 International Geoscience and Remote Sensing Symposium. Taking the Pulse of the Planet: The Role of Remote Sensing in Managing the Environment. Proceedings (Cat. No.00CH37120), 2, 463–466. https://doi.org/10.1109/IGARSS.2000.861597

Hamlet, A. F., Mote, P. W., Clark, M. P., & Lettenmaier, D. P. (2007). Twentieth-Century Trends in Runoff, Evapotranspiration, and Soil Moisture in the Western United States*. Journal of Climate, 20(8), 1468–1486. https://doi.org/10.1175/JCLI4051.1

Hammond, J. C., Saavedra, F. A., & Kampf, S. K. (2018). Global snow zone maps and trends in snow persistence 2001–2016. International Journal of Climatology, 38(12), 4369–4383. https://doi.org/10.1002/joc.5674

Hammond, J. C., Sexstone, G. A., Putman, A. L., Barnhart, T. B., Rey, D. M., Driscoll, J. M., Liston, G. E., Rasmussen, K. L., McGrath, D., Fassnacht, S. R., & Kampf, S. K. (2023). High Resolution SnowModel Simulations Reveal Future Elevation-Dependent Snow Loss and Earlier, Flashier Surface Water Input for the Upper Colorado River Basin. Earth's Future, 11(2), e2022EF003092. https://doi.org/10.1029/2022EF003092

Harshburger, B. J., Humes, K. S., Walden, V. P., Blandford, T. R., Moore, B. C., & Dezzani, R. J. (2010). Spatial interpolation of snow water equivalency using surface observations and remotely sensed images of snow-covered area. Hydrological Processes, 24(10), 1285–1295. https://doi.org/10.1002/hyp.7590

Hedrick, A. R., Marks, D., Havens, S., Robertson, M., Johnson, M., Sandusky, M., Marshall, H., Kormos, P. R., Bormann, K. J., & Painter, T. H. (2018). Direct Insertion of NASA Airborne Snow Observatory-Derived Snow Depth Time Series Into the iSnobal Energy Balance Snow Model. Water Resources Research, 54(10), 8045–8063. https://doi.org/10.1029/2018WR023190

Hunsaker, C. T., Whitaker, T. W., & Bales, R. C. (2012). Snowmelt Runoff and Water Yield Along Elevation and Temperature Gradients in California's Southern Sierra Nevada1. JAWRA Journal of the American Water Resources Association, 48(4), 667–678. https://doi.org/10.1111/j.1752-1688.2012.00641.x

Immerzeel, W. W., Lutz, A. F., Andrade, M., Bahl, A., Biemans, H., Bolch, T., Hyde, S., Brumby, S., Davies, B. J., Elmore, A. C., Emmer, A., Feng, M., Fernández, A., Haritashya, U.,

Kargel, J. S., Koppes, M., Kraaijenbrink, P. D. A., Kulkarni, A. V., Mayewski, P. A., … Baillie, J. E. M. (2020). Importance and vulnerability of the world's water towers. Nature, 577(7790), 364–369. https://doi.org/10.1038/s41586-019-1822-y

Jennings, K. S., Kittel, T. G. F., & Molotch, N. P. (2018). Observations and simulations of the seasonal evolution of snowpack cold content and its relation to snowmelt and the snowpack energy budget. The Cryosphere, 12(5), 1595–1614. https://doi.org/10.5194/tc-12-1595-2018

Jiancheng Shi, & Dozier, J. (1995). Inferring snow wetness using C-band data from SIR-C's polarimetric synthetic aperture radar. IEEE Transactions on Geoscience and Remote Sensing, 33(4), 905–914. https://doi.org/10.1109/36.406676

Jörg-Hess, S., Fundel, F., Jonas, T., & Zappa, M. (2014). Homogenisation of a gridded snow water equivalent climatology for Alpine terrain: Methodology and applications. The Cryosphere, 8(2), 471–485. https://doi.org/10.5194/tc-8-471-2014

Juras, R., Blöcher, J. R., Jenicek, M., Hotovy, O., & Markonis, Y. (2021). What affects the hydrological response of rain-on-snow events in low-altitude mountain ranges in Central Europe? Journal of Hydrology, 603, 127002. https://doi.org/10.1016/j.jhydrol.2021.127002

Kapnick, S., & Hall, A. (2010). Observed Climate–Snowpack Relationships in California and their Implications for the Future. Journal of Climate, 23(13), 3446–3456. https://doi.org/10.1175/2010JCLI2903.1

Kattelmann, R., & Dozier, J. (1999). Observations of snowpack ripening in the Sierra Nevada, California, U.S.A. Journal of Glaciology, 45(151), 409–416. https://doi.org/10.3189/S002214300000126X

Katz, L., Lewis, G., Krogh, S., Drake, S., Hanan, E., Hatchett, B., & Harpold, A. (2023). Antecedent Snowpack Cold Content Alters the Hydrologic Response to Extreme Rain-on-Snow Events. Journal of Hydrometeorology, 24(10), 1825–1846. https://doi.org/10.1175/JHM-D-22-0090.1

Kiewiet, L., Trujillo, E., Hedrick, A., Havens, S., Hale, K., Seyfried, M., Kampf, S., & Godsey, S. E. (2022). Effects of spatial and temporal variability in surface water inputs on streamflow generation and cessation in the rain–snow transition zone. Hydrology and Earth System Sciences, 26(10), 2779–2796. https://doi.org/10.5194/hess-26-2779-2022

Kinar, N. J., & Pomeroy, J. W. (2015). Measurement of the physical properties of the snowpack. Reviews of Geophysics, 53(2), 481–544. https://doi.org/10.1002/2015RG000481

Klein, A. G., Hall, D. K., & Riggs, G. A. (1998). Improving snow cover mapping in forests through the use of a canopy reflectance model. Hydrological Processes, 12(10–11), 1723–1744. https://doi.org/10.1002/(SICI)1099-1085(199808/09)12:10/11<1723::AID-HYP691>3.0.CO;2-2

Kumar, M., Marks, D., Dozier, J., Reba, M., & Winstral, A. (2013). Evaluation of distributed hydrologic impacts of temperature-index and energy-based snow models. Advances in Water Resources, 56, 77–89. https://doi.org/10.1016/j.advwatres.2013.03.006

Laska, M., Luks, B., & Budzik, T. (2016). Influence of snowpack internal structure on snow metamorphism and melting intensity on Hansbreen, Svalbard. Polish Polar Research, 37(2), 193–218. https://doi.org/10.1515/popore-2016-0012

Leathers, K., Herbst, D., De Mendoza, G., Doerschlag, G., & Ruhi, A. (2024). Climate change is poised to alter mountain stream ecosystem processes via organismal phenological shifts. Proceedings of the National Academy of Sciences, 121(14), e2310513121. https://doi.org/10.1073/pnas.2310513121

Li, D., Wrzesien, M. L., Durand, M., Adam, J., & Lettenmaier, D. P. (2017). How much runoff originates as snow in the western United States, and how will that change in the future? Geophysical Research Letters, 44(12), 6163–6172. https://doi.org/10.1002/2017GL073551

Liston, G. E., & Elder, K. (2006). A Distributed Snow-Evolution Modeling System (SnowModel). Journal of Hydrometeorology, 7(6), 1259–1276. https://doi.org/10.1175/JHM548.1

Liston, G. E., & Sturm, M. (2002). Winter Precipitation Patterns in Arctic Alaska Determined from a Blowing-Snow Model and Snow-Depth Observations. Journal of Hydrometeorology, 3(6), 646–659. https://doi.org/10.1175/1525-7541(2002)003<0646:WPPIAA>2.0.CO;2

Liu, H., Xiao, P., Zhang, X., Liang, Y., Tang, B., Chen, S., & Liu, Y. (2024). Winter snowpack loss increases warm-season compound hot-dry extremes. Communications Earth & Environment, 5(1), 567. https://doi.org/10.1038/s43247-024-01734-8

Livneh, B., & Badger, A. M. (2020). Drought less predictable under declining future snowpack. Nature Climate Change, 10(5), 452–458. https://doi.org/10.1038/s41558-020-0754-8

López-Moreno, J. I., Fassnacht, S. R., Heath, J. T., Musselman, K. N., Revuelto, J., Latron, J., Morán-Tejeda, E., & Jonas, T. (2013). Small scale spatial variability of snow density and depth over complex alpine terrain: Implications for estimating snow water equivalent. Advances in Water Resources, 55, 40–52. https://doi.org/10.1016/j.advwatres.2012.08.010

Lund, J., Forster, R. R., Deeb, E. J., Liston, G. E., Skiles, S. M., & Marshall, H.-P. (2022). Interpreting Sentinel-1 SAR Backscatter Signals of Snowpack Surface Melt/Freeze, Warming, and Ripening, through Field Measurements and Physically-Based SnowModel. Remote Sensing, 14(16), 4002. https://doi.org/10.3390/rs14164002

Lund, J., Richard R. Forster, Jameel, Y., Rupper, S. B., Deeb, E. J., Dars, G. H., Zaheer, A., Ali, M., Ghafoor, A., Khan, G., Arfan, M., Liston, G. E., Akhter Qureshi, J., Carling, G., & Burian, S. J. (2023). Constraining Mountain Streamflow Constituents by Integrating Citizen Scientist Acquired Geochemical Samples and Sentinel-1 SAR Wet Snow Time-Series for the Shimshal Catchment in the Karakoram Mountains of Pakistan. Water Resources Research, 59(3), e2022WR032171. https://doi.org/10.1029/2022WR032171

Manickam, S., & Barros, A. (2020). Parsing Synthetic Aperture Radar Measurements of Snow in Complex Terrain: Scaling Behaviour and Sensitivity to Snow Wetness and Landcover. Remote Sensing, 12(3), 483. https://doi.org/10.3390/rs12030483

Marin, C., Bertoldi, G., Premier, V., Callegari, M., Brida, C., Hürkamp, K., Tschiersch, J., Zebisch, M., & Notarnicola, C. (2020). Use of Sentinel-1 radar observations to evaluate snowmelt dynamics in alpine regions. The Cryosphere, 14(3), 935–956. https://doi.org/10.5194/tc-14-935-2020

Marks, D., Domingo, J., Susong, D., Link, T., & Garen, D. (1999). A spatially distributed energy balance snowmelt model for application in mountain basins. Hydrological Processes, 13(12–13), 1935–1959. https://doi.org/10.1002/(SICI)1099-1085(199909)13:12/13<1935::AID-HYP868>3.0.CO;2-C

Marks, D., & Dozier, J. (1992). Climate and energy exchange at the snow surface in the Alpine Region of the Sierra Nevada: 2. Snow cover energy balance. Water Resources Research, 28(11), 3043–3054. https://doi.org/10.1029/92WR01483

Marshall, A. M., & Chen, J. M. (2022). Impacts of changing snowfall on seasonal complementarity of hydroelectric and solar power. Environmental Research: Infrastructure and Sustainability, 2(2), 021001. https://doi.org/10.1088/2634-4505/ac668f

McCabe, G. J., & Clark, M. P. (2005). Trends and Variability in Snowmelt Runoff in the Western United States. Journal of Hydrometeorology, 6(4), 476–482. https://doi.org/10.1175/JHM428.1

Meixner, T., Manning, A. H., Stonestrom, D. A., Allen, D. M., Ajami, H., Blasch, K. W., Brookfield, A. E., Castro, C. L., Clark, J. F., Gochis, D. J., Flint, A. L., Neff, K. L., Niraula, R., Rodell, M., Scanlon, B. R., Singha, K., & Walvoord, M. A. (2016). Implications of projected climate change for groundwater recharge in the western United States. Journal of Hydrology, 534, 124–138. https://doi.org/10.1016/j.jhydrol.2015.12.027

Meromy, L., Molotch, N. P., Link, T. E., Fassnacht, S. R., & Rice, R. (2013). Subgrid variability of snow water equivalent at operational snow stations in the western USA. Hydrological Processes, 27(17), 2383–2400. https://doi.org/10.1002/hyp.9355

Metcalfe, R. A., & Buttle, J. M. (1998). A statistical model of spatially distributed snowmelt rates in a boreal forest basin. Hydrological Processes, 12(10–11), 1701–1722. https://doi.org/10.1002/(SICI)1099-1085(199808/09)12:10/11<1701::AID-HYP690>3.0.CO;2-D

Meybeck, M., Green, P., & Vörösmarty, C. (2001). A New Typology for Mountains and Other Relief Classes: An Application to Global Continental Water Resources and Population Distribution. Mountain Research and Development, 21(1), 34–45. https://doi.org/10.1659/0276-4741(2001)021[0034:ANTFMA]2.0.CO;2

Meyer, J., Horel, J., Kormos, P., Hedrick, A., Trujillo, E., & Skiles, S. M. (2023). Operational water forecast ability of the HRRR-iSnobal combination: An evaluation to adapt into production environments. Geoscientific Model Development, 16(1), 233–250. https://doi.org/10.5194/gmd-16-233-2023

Microsoft Open Source, Matt McFarland, Rob Emanuele, Dan Morris, & Tom Augspurger. (2022). microsoft/PlanetaryComputer: October 2022 (2022.10.28). Zenodo. https://doi.org/10.5281/zenodo.7261897

Mizukami, N., & Perica, S. (2008). Spatiotemporal Characteristics of Snowpack Density in the Mountainous Regions of the Western United States. Journal of Hydrometeorology, 9(6), 1416–1426. https://doi.org/10.1175/2008JHM981.1

Mock, C. J., & Birkeland, K. W. (2000). Snow Avalanche Climatology of the Western United States Mountain Ranges. Bulletin of the American Meteorological Society, 81(10), 2367–2392. https://doi.org/10.1175/1520-0477(2000)081<2367:SACOTW>2.3.CO;2

Molotch, N. P., & Bales, R. C. (2005). Scaling snow observations from the point to the grid element: Implications for observation network design. Water Resources Research, 41(11), 2005WR004229. https://doi.org/10.1029/2005WR004229

Morán-Tejeda, E., López-Moreno, J., Stoffel, M., & Beniston, M. (2016). Rain-on-snow events in Switzerland: Recent observations and projections for the 21st century. Climate Research, 71(2), 111–125. https://doi.org/10.3354/cr01435

Mote, P. W., Hamlet, A. F., Clark, M. P., & Lettenmaier, D. P. (2005). DECLINING MOUNTAIN SNOWPACK IN WESTERN NORTH AMERICA*. Bulletin of the American Meteorological Society, 86(1), 39–50. https://doi.org/10.1175/BAMS-86-1-39

Mote, P. W., Li, S., Lettenmaier, D. P., Xiao, M., & Engel, R. (2018). Dramatic declines in snowpack in the western US. Npj Climate and Atmospheric Science, 1(1), 2. https://doi.org/10.1038/s41612-018-0012-1

Mower, R., Gutmann, E. D., Liston, G. E., Lundquist, J., & Rasmussen, S. (2024). Parallel SnowModel (v1.0): A parallel implementation of a distributed snow-evolution modeling system (SnowModel). Geoscientific Model Development, 17(10), 4135–4154. https://doi.org/10.5194/gmd-17-4135-2024

Musselman, K. N., Addor, N., Vano, J. A., & Molotch, N. P. (2021). Winter melt trends portend widespread declines in snow water resources. Nature Climate Change, 11(5), 418–424. https://doi.org/10.1038/s41558-021-01014-9

Musselman, K. N., Molotch, N. P., & Margulis, S. A. (2017). Snowmelt response to simulated warming across a large elevation gradient, southern Sierra Nevada, California. The Cryosphere, 11(6), 2847–2866. https://doi.org/10.5194/tc-11-2847-2017

Nagler, T., Rott, H., Ripper, E., Bippus, G., & Hetzenecker, M. (2016). Advancements for Snowmelt Monitoring by Means of Sentinel-1 SAR. Remote Sensing, 8(4), 348. https://doi.org/10.3390/rs8040348

Neiman, P. J., Ralph, F. M., Wick, G. A., Lundquist, J. D., & Dettinger, M. D. (2008). Meteorological Characteristics and Overland Precipitation Impacts of Atmospheric Rivers Affecting the West Coast of North America Based on Eight Years of SSM/I Satellite

Observations. Journal of Hydrometeorology, 9(1), 22–47. https://doi.org/10.1175/2007JHM855.1

Newton, B. W., Farjad, B., & Orwin, J. F. (2021). Spatial and Temporal Shifts in Historic and Future Temperature and Precipitation Patterns Related to Snow Accumulation and Melt Regimes in Alberta, Canada. Water, 13(8), 1013. https://doi.org/10.3390/w13081013

Nolin, A. W. (2010). Recent advances in remote sensing of seasonal snow. Journal of Glaciology, 56(200), 1141–1150. https://doi.org/10.3189/002214311796406077

Nolin, A. W., & Daly, C. (2006). Mapping "At Risk" Snow in the Pacific Northwest. Journal of Hydrometeorology, 7(5), 1164–1171. https://doi.org/10.1175/JHM543.1

Oerlemans, J. (Ed.). (1989). Glacier Fluctuations and Climatic Change (Vol. 6). Springer Netherlands. https://doi.org/10.1007/978-94-015-7823-3

Osterhuber, R. (2014). Snow Survey Procedure Manual. The Resources Agency of California.

Oveisgharan, S., Zinke, R., Hoppinen, Z., & Marshall, H. P. (2024). Snow water equivalent retrieval over Idaho – Part 1: Using Sentinel-1 repeat-pass interferometry. The Cryosphere, 18(2), 559–574. https://doi.org/10.5194/tc-18-559-2024

Painter, T. H., Berisford, D. F., Boardman, J. W., Bormann, K. J., Deems, J. S., Gehrke, F., Hedrick, A., Joyce, M., Laidlaw, R., Marks, D., Mattmann, C., McGurk, B., Ramirez, P., Richardson, M., Skiles, S. M., Seidel, F. C., & Winstral, A. (2016). The Airborne Snow Observatory: Fusion of scanning lidar, imaging spectrometer, and physically-based modeling for mapping snow water equivalent and snow albedo. Remote Sensing of Environment, 184, 139–152. https://doi.org/10.1016/j.rse.2016.06.018

Palomaki, R. T., & Sproles, E. A. (2023). Assessment of L-band InSAR snow estimation techniques over a shallow, heterogeneous prairie snowpack. Remote Sensing of Environment, 296, 113744. https://doi.org/10.1016/j.rse.2023.113744

Pomeroy, J. W., Bewley, D. S., Essery, R. L. H., Hedstrom, N. R., Link, T., Granger, R. J., Sicart, J. E., Ellis, C. R., & Janowicz, J. R. (2006). Shrub tundra snowmelt. Hydrological Processes, 20(4), 923–941. https://doi.org/10.1002/hyp.6124

Qin, Y., Abatzoglou, J. T., Siebert, S., Huning, L. S., AghaKouchak, A., Mankin, J. S., Hong, C., Tong, D., Davis, S. J., & Mueller, N. D. (2020). Agricultural risks from changing snowmelt. Nature Climate Change, 10(5), 459–465. https://doi.org/10.1038/s41558-020-0746-8

Rango, A., & Martinec, J. (1995). Revisiting the Degree-Day Method for Snowmelt Computations. JAWRA Journal of the American Water Resources Association, 31(4), 657–669. https://doi.org/10.1111/j.1752-1688.1995.tb03392.x

Revuelto, J., Jonas, T., & López-Moreno, J. (2016). Backward snow depth reconstruction at high spatial resolution based on time-lapse photography. Hydrological Processes, 30(17), 2976–2990. https://doi.org/10.1002/hyp.10823

Revuelto, J., López-Moreno, J. I., Azorin-Molina, C., & Vicente-Serrano, S. M. (2014). Topographic control of snowpack distribution in a small catchment in the central Spanish Pyrenees: Intra- and inter-annual persistence. The Cryosphere, 8(5), 1989–2006. https://doi.org/10.5194/tc-8-1989-2014

Rittger, K., Raleigh, M. S., Dozier, J., Hill, A. F., Lutz, J. A., & Painter, T. H. (2020). Canopy Adjustment and Improved Cloud Detection for Remotely Sensed Snow Cover Mapping. Water Resources Research, 56(6), e2019WR024914. https://doi.org/10.1029/2019WR024914

Robock, A. (1983). Ice and Snow Feedbacks and the Latitudinal and Seasonal Distribution of Climate Sensitivity. Journal of the Atmospheric Sciences, 40(4), 986–997. https://doi.org/10.1175/1520-0469(1983)040<0986:IASFAT>2.0.CO;2

Roth, T. R., & Nolin, A. W. (2017). Forest impacts on snow accumulation and ablation across an elevation gradient in a temperate montane environment. Hydrology and Earth System Sciences, 21(11), 5427–5442. https://doi.org/10.5194/hess-21-5427-2017

Roy, A., Toose, P., Williamson, M., Rowlandson, T., Derksen, C., Royer, A., Berg, A. A., Lemmetyinen, J., & Arnold, L. (2017). Response of L-Band brightness temperatures to freeze/thaw and snow dynamics in a prairie environment from ground-based radiometer measurements. Remote Sensing of Environment, 191, 67–80. https://doi.org/10.1016/j.rse.2017.01.017

Ruiz, J. J., Lemmetyinen, J., Kontu, A., Tarvainen, R., Vehmas, R., Pulliainen, J., & Praks, J. (2022). Investigation of Environmental Effects on Coherence Loss in SAR Interferometry for Snow Water Equivalent Retrieval. IEEE Transactions on Geoscience and Remote Sensing, 60, 1–15. https://doi.org/10.1109/TGRS.2022.3223760

Sarmiento, F. O. (Ed.). (2022). Montology Palimpsest: A Primer of Mountain Geographies (Vol. 1). Springer International Publishing. https://doi.org/10.1007/978-3-031-13298-8

Schwank, M., & Naderpour, R. (2018). Snow Density and Ground Permittivity Retrieved from L-Band Radiometry: Melting Effects. Remote Sensing, 10(2), 354. https://doi.org/10.3390/rs10020354

Seibert, J., Jenicek, M., Huss, M., Ewen, T., & Viviroli, D. (2021). Snow and ice in the hydrosphere. In Snow and Ice-Related Hazards, Risks, and Disasters (pp. 93–135). Elsevier. https://doi.org/10.1016/B978-0-12-817129-5.00010-X

Serreze, M. C., Clark, M. P., Armstrong, R. L., McGinnis, D. A., & Pulwarty, R. S. (1999). Characteristics of the western United States snowpack from snowpack telemetry (SNOTEL) data. Water Resources Research, 35(7), 2145–2160. https://doi.org/10.1029/1999WR900090

Siirila-Woodburn, E. R., Rhoades, A. M., Hatchett, B. J., Huning, L. S., Szinai, J., Tague, C., Nico, P. S., Feldman, D. R., Jones, A. D., Collins, W. D., & Kaatz, L. (2021). A low-to-no snow future and its impacts on water resources in the western United States. Nature Reviews Earth & Environment, 2(11), 800–819. https://doi.org/10.1038/s43017-021-00219-y

Sourp, L., Gascoin, S., Jarlan, L., Pedinotti, V., Bormann, K. J., & Baba, M. W. (2025). Evaluation of high-resolution snowpack simulations from global datasets and comparison with Sentinel-1 snow depth retrievals in the Sierra Nevada, USA. Hydrology and Earth System Sciences, 29(3), 597–611. https://doi.org/10.5194/hess-29-597-2025

Space Studies Board, Division on Engineering and Physical Sciences, & National Academies of Sciences, Engineering, and Medicine. (2019). Thriving on Our Changing Planet: A Decadal Strategy for Earth Observation from Space: An Overview for Decision Makers and the Public (p. 25437). National Academies Press. https://doi.org/10.17226/25437

Sproles, E. A., Nolin, A. W., Rittger, K., & Painter, T. H. (2013). Climate change impacts on maritime mountain snowpack in the Oregon Cascades. Hydrology and Earth System Sciences, 17(7), 2581–2597. https://doi.org/10.5194/hess-17-2581-2013

Stewart, I. T. (2009). Changes in snowpack and snowmelt runoff for key mountain regions. Hydrological Processes, 23(1), 78–94. https://doi.org/10.1002/hyp.7128

Stewart, I. T., Cayan, D. R., & Dettinger, M. D. (2004). Changes in Snowmelt Runoff Timing in Western North America under a `Business as Usual' Climate Change Scenario. Climatic Change, 62(1–3), 217–232. https://doi.org/10.1023/B:CLIM.0000013702.22656.e8

Sturm, M., Goldstein, M. A., & Parr, C. (2017). Water and life from snow: A trillion dollar science question. Water Resources Research, 53(5), 3534–3544. https://doi.org/10.1002/2017WR020840

Sturm, M., & Holmgren, J. (1998). Differences in compaction behavior of three climate classes of snow. Annals of Glaciology, 26, 125–130. https://doi.org/10.3189/1998AoG26-1-125-130

Sturm, M., Holmgren, J., & Liston, G. E. (1995). A seasonal snow cover classification system for local to global applications. *Journal of climate*, *8*(5), 1261-1283.

Sturm, M., & Liston, G. E. (2021). Revisiting the Global Seasonal Snow Classification: An Updated Dataset for Earth System Applications. Journal of Hydrometeorology. https://doi.org/10.1175/JHM-D-21-0070.1

Tarricone, J., Webb, R. W., Marshall, H.-P., Nolin, A. W., & Meyer, F. J. (2023). Estimating snow accumulation and ablation with L-band interferometric synthetic aperture radar (InSAR). The Cryosphere, 17(5), 1997–2019. https://doi.org/10.5194/tc-17-1997-2023

Trujillo, E., & Molotch, N. P. (2014). Snowpack regimes of the Western United States. Water Resources Research, 50(7), 5611–5623. https://doi.org/10.1002/2013WR014753

Trujillo, E., Ramírez, J. A., & Elder, K. J. (2007). Topographic, meteorologic, and canopy controls on the scaling characteristics of the spatial distribution of snow depth fields. Water Resources Research, 43(7), 2006WR005317. https://doi.org/10.1029/2006WR005317

Tsang, L., Durand, M., Derksen, C., Barros, A. P., Kang, D.-H., Lievens, H., Marshall, H.-P., Zhu, J., Johnson, J., King, J., Lemmetyinen, J., Sandells, M., Rutter, N., Siqueira, P., Nolin, A., Osmanoglu, B., Vuyovich, C., Kim, E., Taylor, D., … Xu, X. (2022). Review article: Global

monitoring of snow water equivalent using high-frequency radar remote sensing. The Cryosphere, 16(9), 3531–3573. https://doi.org/10.5194/tc-16-3531-2022

United States Geological Survey (2021). United States Geological Survey 3D Elevation Program 1/3 arc-second Digital Elevation Model. Distributed by OpenTopography. https://doi.org/10.5069/G98K778D. Accessed: 2025-03-28

U.S. Environmental Protection Agency. (2013). Level III ecoregions of the conterminous United States [Dataset]. U.S. EPA Office of Research and Development, National Health and Environmental Effects Research Laboratory. Retrieved from https://www.epa.gov/eco-research/level-iii-and-iv-ecoregions-continental-united-states

USDA NRCS. (2024). SNOwpack TELemetry Network (SNOTEL) [Dataset]. USDA NRCS. Retrieved from https://catalog.data.gov/dataset/snowpack-telemetry-network-snotel

Uzun, S., Tanir, T., Coelho, G. D. A., Souza De Lima, A. D., Cassalho, F., & Ferreira, C. M. (2021). Changes in snowmelt runoff timing in the contiguous United States. Hydrological Processes, 35(11), e14430. https://doi.org/10.1002/hyp.14430

Vavrus, S. (2007). The role of terrestrial snow cover in the climate system. Climate Dynamics, 29(1), 73–88. https://doi.org/10.1007/s00382-007-0226-0

Viviroli, D., Dürr, H. H., Messerli, B., Meybeck, M., & Weingartner, R. (2007). Mountains of the world, water towers for humanity: Typology, mapping, and global significance. Water Resources Research, 43(7), 2006WR005653. https://doi.org/10.1029/2006WR005653

Wake, L. M., & Marshall, S. J. (2015). Assessment of current methods of positive degree-day calculation using in situ observations from glaciated regions. Journal of Glaciology, 61(226), 329–344. https://doi.org/10.3189/2015JoG14J116

Wang, X., Wang, T., Guo, H., Liu, D., Zhao, Y., Zhang, T., Liu, Q., & Piao, S. (2018). Disentangling the mechanisms behind winter snow impact on vegetation activity in northern ecosystems. Global Change Biology, 24(4), 1651–1662. https://doi.org/10.1111/gcb.13930

Warren, S. G. (1982). Optical properties of snow. Reviews of Geophysics, 20(1), 67–89. https://doi.org/10.1029/RG020i001p00067

Webb, R. W., Fassnacht, S. R., & Gooseff, M. N. (2018). Hydrologic flow path development varies by aspect during spring snowmelt in complex subalpine terrain. The Cryosphere, 12(1), 287–300. https://doi.org/10.5194/tc-12-287-2018

Webb, R. W., Musselman, K. N., Ciafone, S., Hale, K. E., & Molotch, N. P. (2022). Extending the vadose zone: Characterizing the role of snow for liquid water storage and transmission in streamflow generation. Hydrological Processes, 36(3), e14541. https://doi.org/10.1002/hyp.14541

Webb, R. W., Raleigh, M. S., McGrath, D., Molotch, N. P., Elder, K., Hiemstra, C., Brucker, L., & Marshall, H. P. (2020). Within-Stand Boundary Effects on Snow Water Equivalent

Distribution in Forested Areas. Water Resources Research, 56(10). https://doi.org/10.1029/2019WR024905

Wetlaufer, K., Hendrikx, J., & Marshall, L. (2016). Spatial Heterogeneity of Snow Density and Its Influence on Snow Water Equivalence Estimates in a Large Mountainous Basin. Hydrology, 3(1), 3. https://doi.org/10.3390/hydrology3010003

Wrzesien, M. L., Durand, M. T., Pavelsky, T. M., Kapnick, S. B., Zhang, Y., Guo, J., & Shum, C. K. (2018). A New Estimate of North American Mountain Snow Accumulation From Regional Climate Model Simulations. Geophysical Research Letters, 45(3), 1423–1432. https://doi.org/10.1002/2017GL076664

Yu, Y., Zhou, Y., Li, M., Xue, W., Liu, J., & Hu, Y. (2024). Elevation-dependent effects of snowfall and snow cover changes on runoff variations at the source regions of the Yellow River basin. Journal of Water and Climate Change, 15(8), 3566–3581. https://doi.org/10.2166/wcc.2024.658

Zanaga, D., Van De Kerchove, R., De Keersmaecker, W., Souverijns, N., Brockmann, C., Quast, R., Wevers, J., Grosu, A., Paccini, A., Vergnaud, S., Cartus, O., Santoro, M., Fritz, S., Georgieva, I., Lesiv, M., Carter, S., Herold, M., Li, L., Tsendbazar, N.-E., … Arino, O. (2021). ESA WorldCover 10 m 2020 v100 (Version v100) [Dataset]. Zenodo. https://doi.org/10.5281/zenodo.5571936

Zeng, X., Broxton, P., & Dawson, N. (2018). Snowpack Change From 1982 to 2016 Over Conterminous United States. Geophysical Research Letters, 45(23). https://doi.org/10.1029/2018GL079621

Zhao, W., Mu, C., Han, L., Sun, W., Sun, Y., & Zhang, T. (2023). Spatial and temporal variability in snow density across the Northern Hemisphere. CATENA, 232, 107445. https://doi.org/10.1016/j.catena.2023.107445